

Figure 3.2-22 PCD Pulse Pressure and Face Velocity, September 11, 2001 Through September 18, 2001

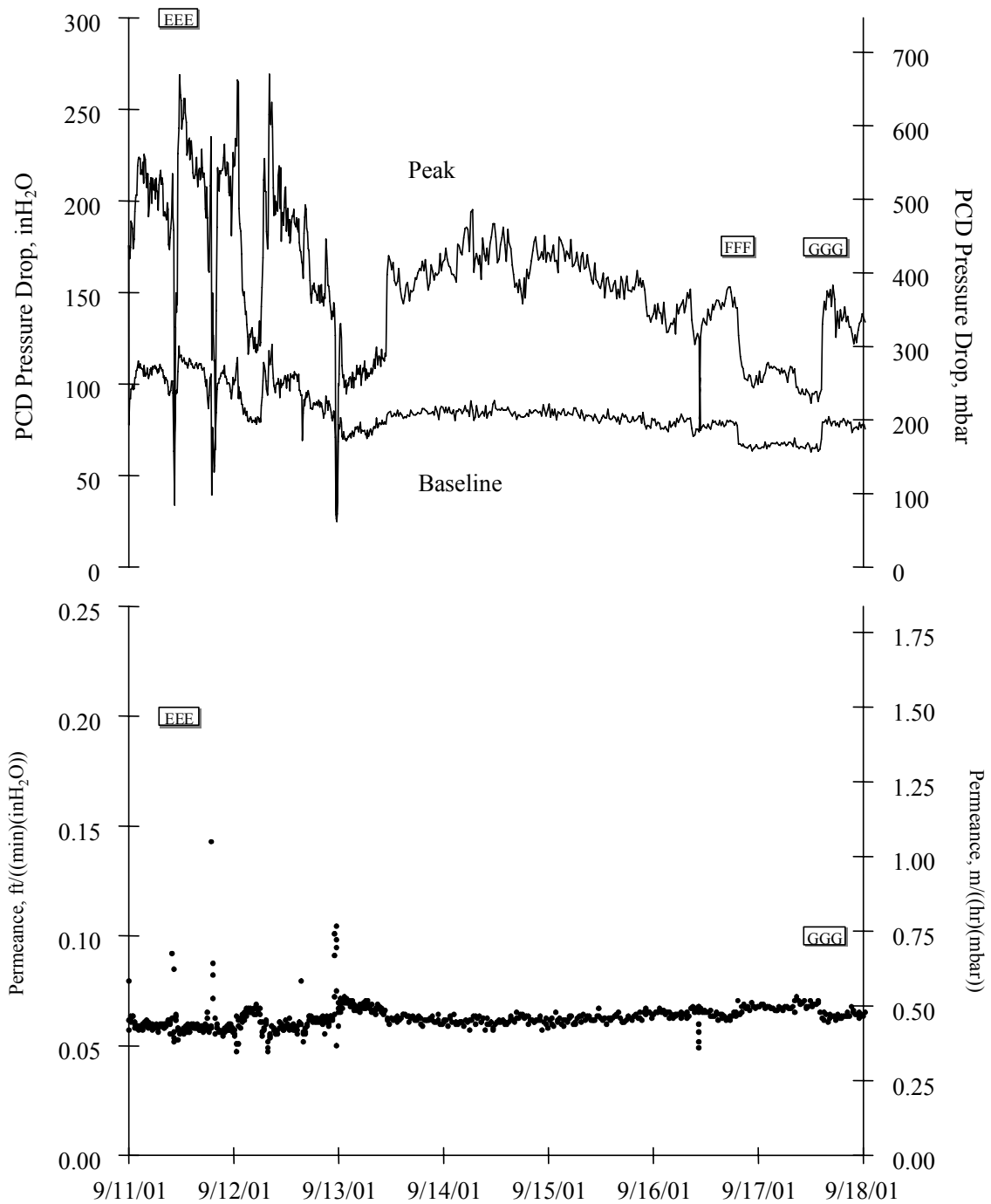


Figure 3.2-23 PCD Pressure Drop and Permeance, September 11, 2001 Through September 18, 2001

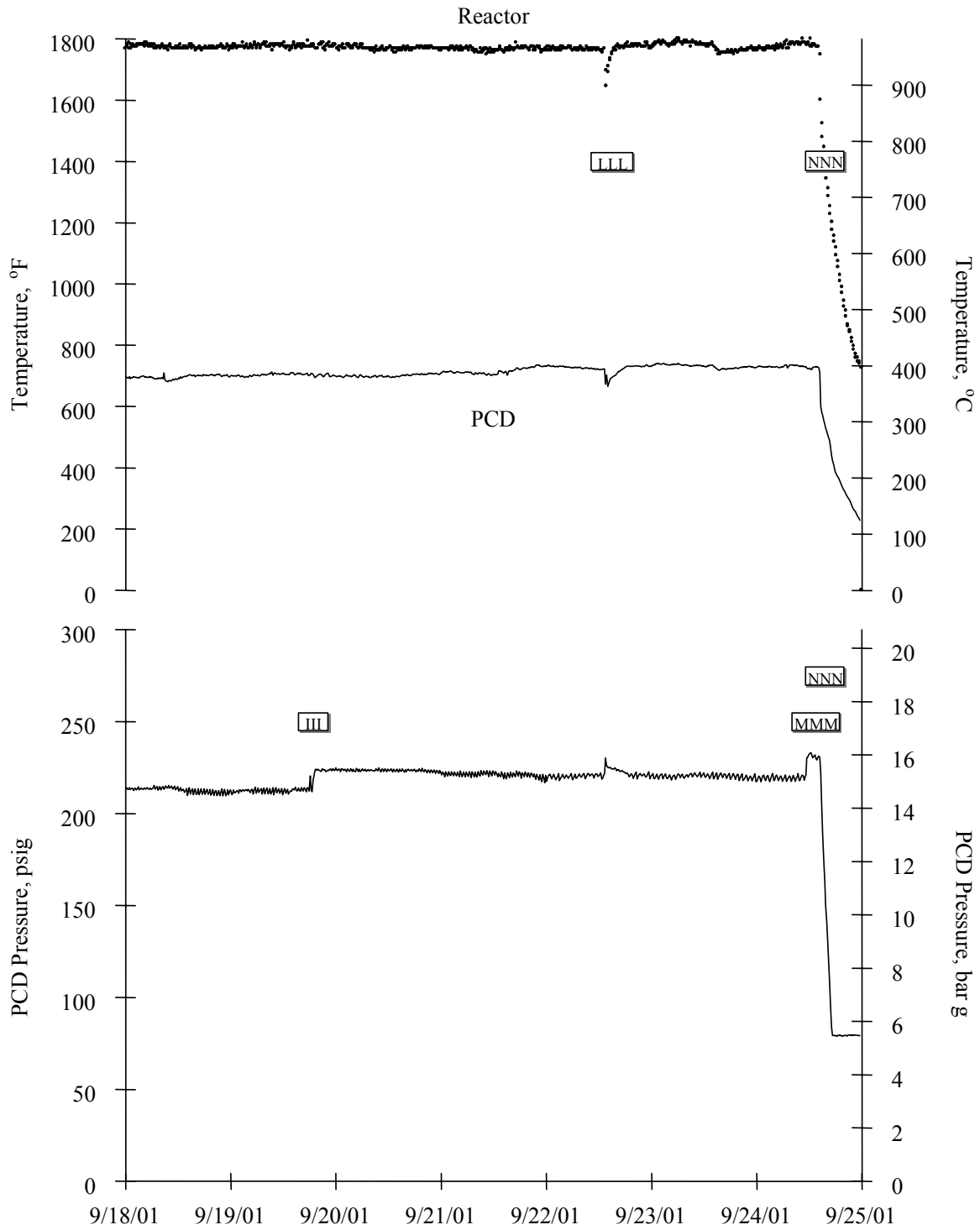


Figure 3.2-24 Reactor and PCD Temperatures and PCD Pressure, September 18, 2001 Through September 25, 2001

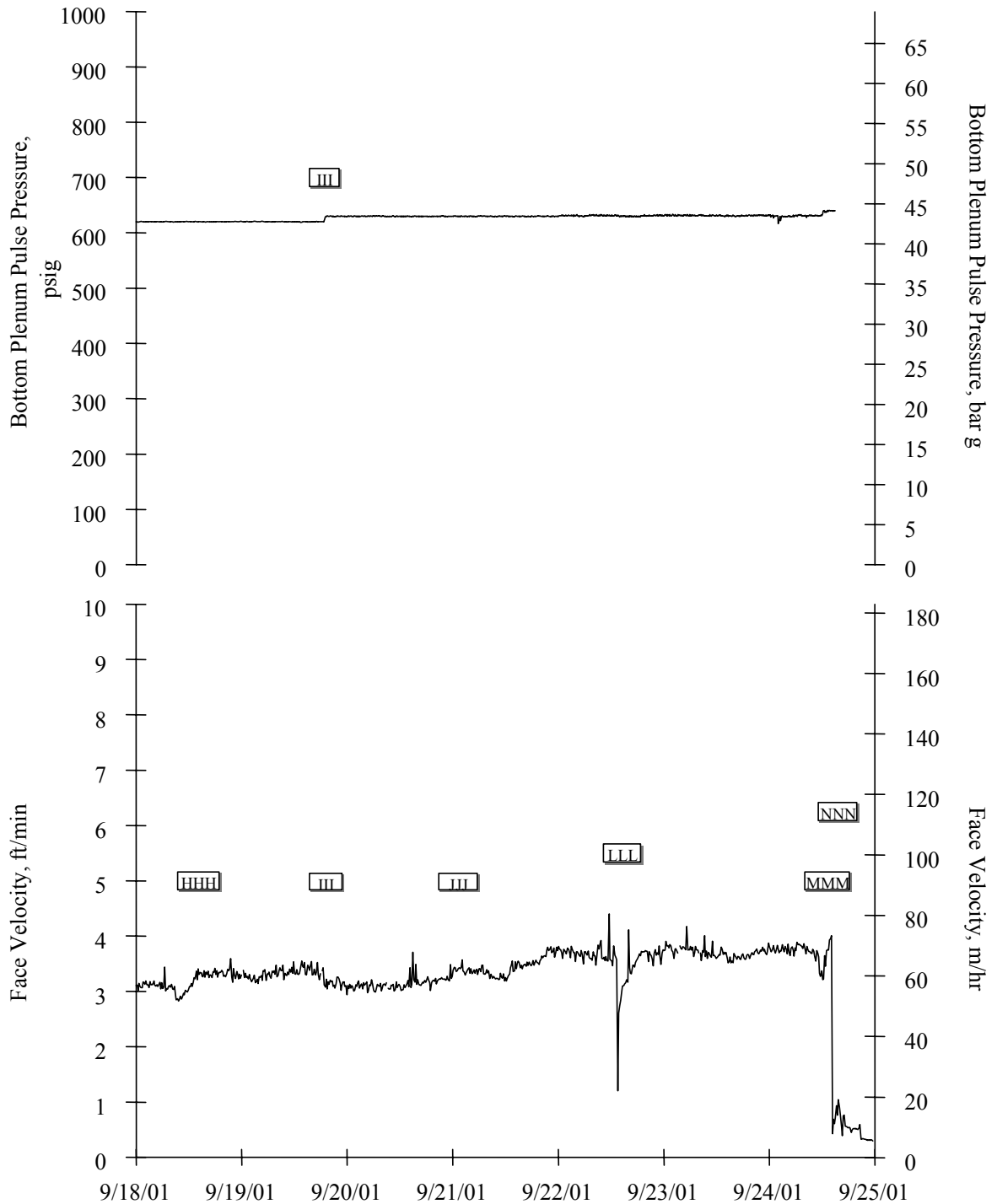


Figure 3.2-25 PCD Pulse Pressure and Face Velocity, September 18, 2001 Through September 25, 2001

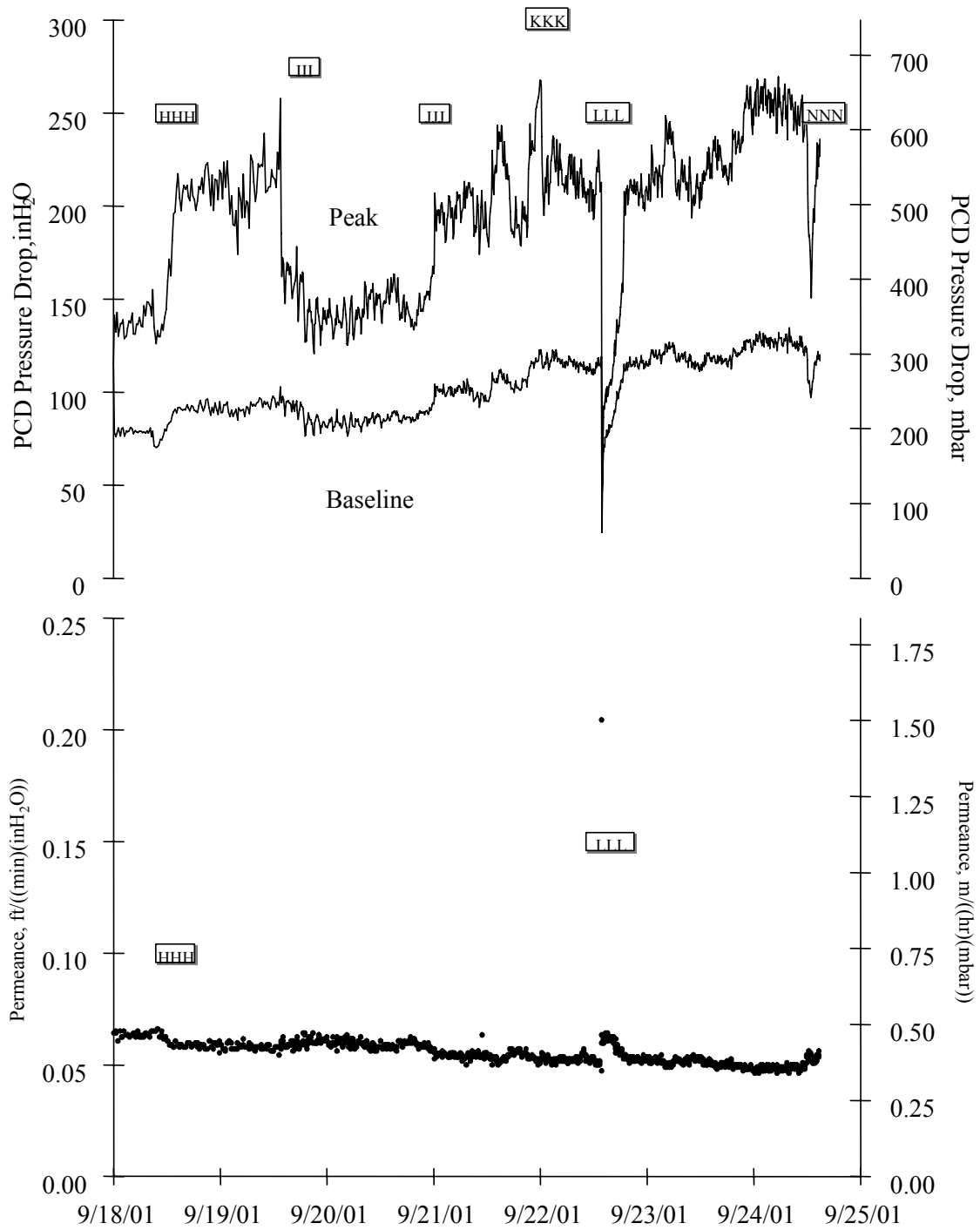


Figure 3.2-26 PCD Pressure Drop and Permeance, September 18, 2001 Through September 25, 2001

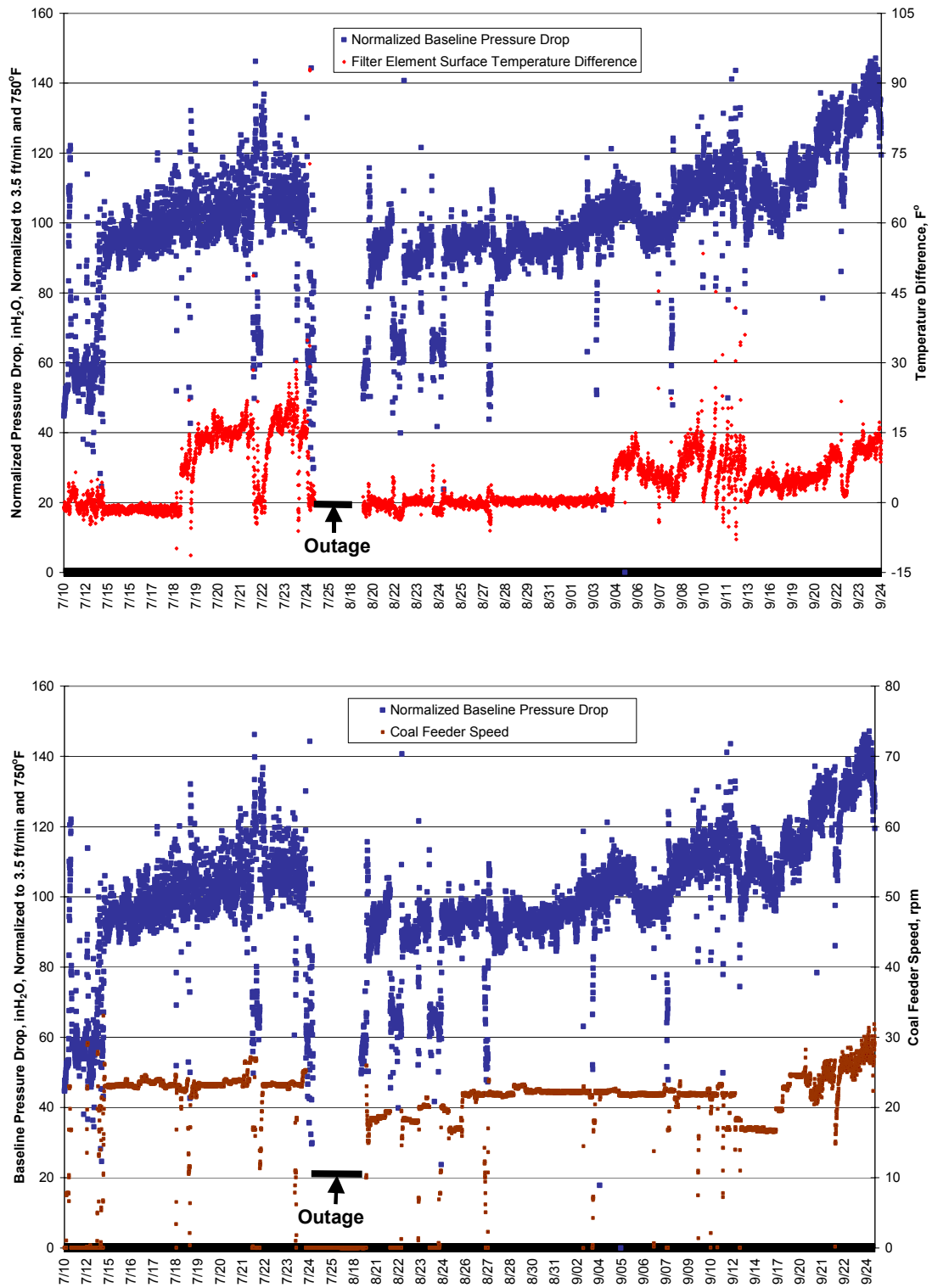


Figure 3.2-27 Normalized Pressure Drop, Filter Surface Temperature Difference, and Coal Feeder Speed

3.3 TC06 INSPECTION REPORT

3.3.1 Introduction

The TC06 test run was divided into two components, TC06A and TC06B. For the PCD, TC06A started on July 6, 2001, and ended on July 25, 2001. During TC06A, the PCD operated approximately 228 on-coal hours. TC06B started on August 18, 2001, and ended on September 24, 2001. During TC06B, the PCD operated approximately 797 on-coal hours. During the TC06 test run, the PCD was exposed to a total of 1,025 on-coal hours. Outage inspections were conducted after both TC06A and TC06B and included examinations of the filter elements, their fixtures to the plenums, solids deposition, filter element gaskets, and auxiliary equipment. This inspection report is divided in two sections. The first section addresses the outage activity after TC06A; while the second section addresses the outage activity after TC06B.

3.3.2 TC06A Inspection

The PCD operated in gasification mode for approximately 228 on-coal hours during TC06A. The PCD operating parameters for TC06A are shown in [Table 3.3-1](#). The outlet loading from the PCD, as measured by SRI, was below 1 ppmw before July 25, 2001. On July 25 SRI measured an outlet loading of approximately 23 ppmw in an off-coal period. The main air compressor was tuned online on July 24, 2001. Oxygen broke through to the PCD and ignited the gasification ash (g-ash) while the air compressor was being tuned. It was believed that one or more filters had failed; therefore, the run was terminated to prevent contamination of unaffected filters by backside blinding. The purpose of this shutdown was to replace the broken filter or filters and start the run again as quickly as possible; therefore, the solids removal system was not inspected.

The PCD was shut down clean, which means the back-pulse system continued to cycle after the coal feed was stopped. The PCD vessel was opened on July 27, 2001. Upon inspection, one filter element was discovered cracked and several were bowed. Based on these findings it was decided to remove 15 filters from the affected area.

3.3.2.1 TC06A Filter Elements

The following filter elements were installed for TC06A: 54 Pall 1.5-meter Fe₃Al; 23 Pall 1.5-meter Fe₃Al with fuse; 5 Pall 2-meter Fe₃Al; 1 Pall 2-meter Fe₃Al with fuse; 5 Pall 1.5-meter Hastelloy X; and 2 U.S. Filter 1.5-meter sintered metal fiber filters (See [Figure 3.3-1](#)). The fuse is a safeguard device inserted into the clean side of the filter. In the event of a filter failure the fuse acts as a backup filter.

As mentioned in the Section 3.2, TC06A was ended due to a filter leak. On July 24, 2001, the main air compressor was tuned while online; however, the coal feed was stopped. Originally, it was believed that oxygen would not ignite the g-ash at low temperature. The temperature in the PCD during this time was below 500°F. Around 16:20 on July 24, 2001, the temperature measured by thermocouple TI3025N (B-53) began to increase rapidly after the air compressor tuning began (See [Figure 3.3-2](#)). [Figure 3.3-2](#) shows that the temperature measured by this

thermocouple reached approximately 810°F, significantly higher than the inlet gas temperature; therefore, localized combustion was suspected. Figures 3.3-2 and -3 show that TI3025N (B-53) and TI3025J (B-15) were the only two thermocouples that showed a significant response. These thermocouples show the temperature at a single point but it is suspected that the elements reached higher temperatures. Figure 3.3-1 shows that these two filters (B-53 and B-15) were in the same area; therefore, g-ash bridging in that area was suspected. G-ash bridging has been noticed in this area in past run inspections. Also, starting on July 19, 2001, TI3025N and TI3025J began reading temperatures that were different from the other thermocouples on the lower plenum. It is believed that this indicated that these two thermocouples were covered with g-ash; however, the mechanism to explain the different temperatures is not fully understood. After this thermal event the on-line particulate monitor (PCME) indicated a possible leak. SRI verified that there was a leak by taking an outlet sample. The sample revealed that the outlet loading was ~ 23 ppmw. At this point the run was terminated to prevent filter contamination from the backside.

On July 27, 2001, the PCD plenum was removed for inspection. Upon inspection a crack was found near the weld between the top and middle sections of Pall Fe₃Al Element 21076, location B-32 (See Figure 3.3-4). This filter was located in the area where the temperature spike was detected by thermocouples TI3025N and TI3025J. When the support brackets were removed from the bottom of this element and the ones around it, as required for its removal, it became apparent that several elements were bowed (See Figure 3.3-5). The support brackets were then removed from all elements on the bottom plenum to determine how many elements were bowed. Five bowed elements were found, all in the same area and all of the bowed elements were apparently exposed to the temperature spike (See Figure 3.3-6). These five elements were removed and replaced for TC06B. Since the extent of the suspected g-ash bridging and subsequent damage to the filters was not known, 15 filters were removed during this outage. The locations of the elements that were removed are shown in Figure 3.3-6.

After removal, the elements were cleaned by water washing and then inspected. On inspection, a dramatic color pattern was seen. The elements were light colored on one side and bowed toward that side (See Figures 3.3-7 and -8). The light color resulted from combustion of bridged g-ash on the surface of the elements; therefore, these regions reached the highest temperature during the thermal transient. The bowing of the Fe₃Al elements and the failure of the element at location B-32 can be understood from the thermal expansion of this material measured in the SRI lab. Thermal expansion up to 2,100°F, measured during heating up from room temperature and then cooling down, is shown in Figure 3.3-9. In this plot, the change in length divided by original length (that is, the unit thermal expansion) is plotted on the y-axis and temperature on the x-axis. The slope of this curve is the familiar coefficient of thermal expansion. At approximately 1,800°F, the curve measured during heating begins to “roll over.” This behavior in thermal expansion is usually an indication of a change in the material such as a phase change. In fact, the Al-Fe phase diagram indicates that a phase change occurs at approximately 1,800°F, the exact temperature depending on the composition. The thermal expansion curve obtained during cooling (Figure 3.3-9) is offset below the curve obtained during heatup. The implication of this is that after the material underwent the phase change at 1,800°F the length was permanently decreased. During the thermal transient of TC06A, one side of the elements (the light-colored side) got hot enough to go through the phase change and the length was permanently changed. The other side did not. Therefore, on cool down after thermal transient,

the elements tended to bow to accommodate the different lengths resulting from one side of the elements undergoing a phase change but not the other side. Since the bottom supports restrained the elements from bowing, one of them failed.

Other than the one failed element and the bowed elements, the Pall Fe₃Al filters performed well during the TC06A gasification run. The remaining Fe₃Al elements were inspected and no obvious damage was found. At this point some of the filters had accumulated 669 on-coal hours while being exposed during GCT3, GCT4, and TC06A.

Five Pall Hastelloy X filters were tested for the first time since GCT1A. During GCT1A the PCD was operating at higher temperatures (> 900°F). There was concern that the nickel in the filter material would react with the sulfur in the gas at these temperatures and form nickel-sulfide, which would ultimately blind the filter. Since the temperatures were constantly below 800°F during GCT3 and GCT4 it was decided to start testing the Pall Hastelloy X filters again. Each filter was visually inspected and no obvious damage was found.

Currently, the PSDF is working with U.S. Filter to test new sintered metal fiber filter element materials. Based on their experience with filtration media, U.S. Filter suggested that the following materials be tested:

- Fecralloy-M (FeCrAlY).
- Haynes Alloy 214.
- Haynes Alloy 160.
- Haynes Alloy 230.

Sintered metal fiber elements have lower pressure drops than sintered metal powder elements. Only two filters from U.S. Filter were installed for this run. Each filter was constructed from three separate filter sections. These sections were connected to each other by welding the porous media to solid metal rings. One filter was constructed from Fecralloy-M, while the other filter was constructed with the other three remaining alloys (Haynes 214, 160, and 230). In other words, each section was made from a different alloy. This offered the advantage of screening three different filter materials, while using only one filter position. Each filter was visually inspected and no obvious damage was found; therefore, it was decided to continue testing these filters during TC06B.

3.3.2.2 TC06A G-ash Deposition

G-ash bridging was believed to have contributed to the temperature excursion in the PCD; however, upon inspection g-ash bridging was not observed. [Figure 3.3-10](#) shows the bottom plenum being lifted out of the PCD vessel and into the maintenance bay. This figure shows that the filters were relatively clean compared to past gasification runs. During the temperature excursion the bridged material may have dislodged and fallen out or burned out. The material that was left on the filters had a relatively high ash content indicating partial combustion.

The g-ash buildup on the filter element fixtures was light compared to past gasification runs. The g-ash buildup on the top and bottom plenums was not severe. [Figure 3.3-11](#) shows the

accumulated g-ash on the top ash shed. [Figure 3.3-12](#) shows very little g-ash buildup on the inside wall of the shroud. Also, there was very little buildup on the liner sections. The clean side of the tubesheet appeared to be in good shape despite the filter failure. [Figure 3.3-13](#) shows that the insulation on the clean side of the tubesheet was relatively clean. [Figure 3.3-14](#) shows the condition of the insulation in the PCD head. The insulation reveals the g-ash penetration in that area was not significant. The shiny scale material detected in GCT3 and GCT4 was not found after this run. Before this run a coke breeze feeder system was installed to help prevent tar formation. The existing start-up burner on the Transport Reactor can raise the reactor temperature to around 1,000°F. In the past, coal has been fed after the reactor temperature exceeded 1,000°F. While the reactor was heating up to 1,600 from 1,000°F on coal, tars were produced because there was not enough energy to crack them. It is suspected that these tars condense during the back-pulse, leaving the shiny scale that has been noted. The coke breeze is fed to the reactor once the reactor reaches 1,000°F. When the reactor reaches 1,600°F coal is introduced to the reactor and the coke breeze system is shut down. The coke breeze feeder addition appears to have solved the tar formation problem.

3.3.2.3 TC06A Filter Element Gaskets

One of the test objectives for the PCD during TC06A was to continue evaluating the Siemens Westinghouse lapped construction gaskets. These gaskets have performed very well since testing began during GCT1B. The gasket types used during TC06A are:

<u>Gasket Type</u>	<u>Gasket Location</u>	<u>Function</u>
Lapped construction	Plenum-to-failsafe	Sealing
Top donut	Failsafe-to-failsafe holder	Sealing
Bottom donut (No.1)	Failsafe holder-to-element	Sealing
Bottom donut (No.2)	Filter nut-to-element	Nonsealing
Sock gasket	Element-to-bottom donut gasket	Nonsealing

During this outage only 17 filter elements were inspected. Therefore, the inspection of the gaskets was not extensive. However, the following observations were made based on the gaskets that were examined:

- There were no leak paths in the area of the failsafe holder flanges that would indicate a leak past the primary gasket.
- Some lapped construction gaskets had broken fibers. This did not appear to affect the sealing capability of the gasket. It is possible that the fibers were damaged during removal.
- Some of the gaskets were cut to inspect the extent of g-ash penetration. The inside of the sealing gaskets were relatively clean.
- The gaskets above the failed filter were dirty, which was expected.

3.3.2.4 TC06A Failsafes

Thirteen failsafe devices were removed during this outage. Several screens on top of the Siemens Westinghouse designed failsafes were found damaged. The failsafe device that was in the B-52 position had the most damage. There were large holes in the top and bottom screens. There was a large amount of rust on top of the failsafe device. It is believed that the rust came from the carbon steel back-pulse pipes used before the carbon steel pipe was replaced with stainless steel for TC06. The mechanism that caused damage to the failsafe device screens is not understood; therefore, the failsafe above B-52 was sent to Siemens Westinghouse for further inspection.

The failsafe device above the Fe₃Al filter that failed was removed and flow tested. This failsafe was a standard Siemens Westinghouse design. The flow coefficient was 11.2 lb/(hr-(lb/ft³)-inH₂O)^{0.5} compared to an average of 133.7 lb/(hr-(lb/ft³)-inH₂O)^{0.5} for a clean failsafe device; therefore, the flow coefficient of the plugged failsafe was about 8 percent of the clean failsafe value. Based on the flow test values, the Siemens Westinghouse failsafe device appeared to have at least partially plugged; however, as mentioned above the outlet loading after the thermal event was ~23 ppmw. These results imply that failsafe research is still necessary.

3.3.2.5 TC06A Auxiliary Equipment

Prior to TC06, 14 thermocouples were installed on individual filter elements to monitor local temperatures. During this outage all of the thermocouples were tested to check for damage. No damage was detected; therefore, all of the thermocouples were reused. Starting with GCT2 all the thermocouple wires were routed from the dirty side of the PCD directly to atmosphere through a nitrogen purged flange on the PCD. The thermocouple wires were sealed using Conax fittings with Teflon sealant. This arrangement has been successful in all the gasification runs since GCT2. During the outage, the Conax fittings were inspected. They appeared to be in good condition and were reused.

The back-pulse pipes inside the PCD head were also inspected. There was a slight discoloration on the back-pulse pipes; however, there was no tar buildup. The inner line of the back-pulse pipes appeared to be in good condition.

3.3.2.6 TC06A Solids Removal Equipment

Since the solids removal equipment performed well during the first 228 hours of TC06, it was decided to postpone any inspection. During TC06A the screw cooler required very little attention. Periodically, maintenance personnel would tighten down the packing follower to seal minor leaks. Also, the lock-vessel (FD0520) system was not disassembled because it performed well during TC06A with one exception. During startup at the beginning of TC06A the conveying line between FD0520 and FD0530 plugged. During this outage the seal on the spherical valve was tested and it checked out; therefore, it was decided to keep running FD0520 without disassembling the system.

3.3.3 TC06B Inspection

The PCD operated in gasification mode for approximately 797 on-coal hours during TC06B. The PCD parameters for TC06B are shown in [Table 3.3-2](#). The outlet loading from the PCD, as measured by SRI, was less than 1 ppmw throughout TC06B. The PCD was shut down dirty after the coal feed was stopped. This allowed SRI to collect transient dustcake samples. The PCD vessel was opened on September 27, 2001. The initial inspection revealed a large amount of g-ash bridging on the lower plenum. During this outage 34 filter elements were removed.

3.3.3.1 TC06B G-ash Deposition

[Figure 3.3-15](#) shows the severity of the g-ash bridging as the plenum was lifted out of the PCD vessel. Once the plenum was set in the maintenance bay, inspection of the PCD internals continued. The g-ash bridging was isolated to the lower plenum. [Figure 3.3-16](#) is a filter layout that shows where the g-ash bridging was found on the lower plenum. The numbers around the layout designate how far down the length of the filter the g-ash penetrated. [Figure 3.3-17](#) shows the extent of the g-ash bridging in the area of TI3025J. On September 4, 2001, the temperature from this thermocouple began to deviate from the other thermocouples. This relationship between temperature deviation and g-ash bridging has been noticed, but no satisfactory explanation for the temperature deviation has been found.

Since this was the fourth time that g-ash bridging was either detected or suspected during a gasification run, several suggestions to address the g-ash bridging issue were explored. These suggestions included:

- **Install a soot blower:** A soot blower would involve blowing high-pressure nitrogen through nozzles strategically placed immediately below the tubesheet to remove g-ash bridging. A feasibility test was conducted on the g-ash bridging material that was found on the lower plenum after shutdown. A soot blower lance was constructed with a 1/8-inch diameter nozzle that could be directed downward from the top of the g-ash bridge. The high-pressure air (100-psig service air) did not remove the g-ash bridging. It was found that the soot blower was effective in removing the deposit only within about 1 foot of the nozzle exit. Therefore, it was determined that once the g-ash bridging forms it will be difficult to remove with a soot blower. Based on these results it was suggested that the soot blower should be used to prevent the g-ash bridging from ever forming. In other words, a soot blower should be installed and cycled periodically (or continuously) to keep the material from consolidating. However, it was concluded that by preventing the formation of g-ash bridging, a learning opportunity would be missed since the g-ash bridging mechanism is not understood.
- **Remove all 2-meter filter elements:** One possible mechanism that has been suggested for the formation of the g-ash bridge was that the back-pulse gas intensity was not evenly distributed due to the 2-meter filter elements. All six 2-meter filter elements from TC06 will be replaced with 1.5-meter elements for TC07.

- Remove tie wire: Tie wire is currently used to secure the metal filter elements in the event of a filter failure. Originally, there were some concerns that a failed metal filter element would damage the screw cooler (FD0502). Since the filter elements are secured at the bottom by the support pins, the relative risk of filters failing and falling into the screw cooler is low; therefore, the tie wires will be removed for TC07. The thought behind removing the tie wire is to remove any object that would possibly facilitate g-ash bridging.
- Determine how the g-ash bridge forms: Instrumentation to measure the pressure inside the filter elements during TC07 will be installed. Since bridging has consistently been seen in certain areas, test measurements will be made in an area where g-ash bridging has not been detected and an area where g-ash bridging is normally seen. The pressure measurements will be made inside the filter element to test this theory of preferential flow during a back-pulse. In addition to pressure measurements, thermocouples will be inserted into the filter elements to monitor the temperature. Also, before TC07, 12 additional thermocouples will be installed. Currently, the PCD divides 14 thermocouples evenly between the top and bottom plenums. For TC07, 3 thermocouples will be installed on the top plenum and the remaining 23 thermocouples will be installed on the bottom plenum. The purpose for these thermocouples is to determine where the g-ash bridging originates.
- Maintain constant back-pulse timer and test higher back-pulse pressures: During the next run the back-pulse time interval will be set and maintained at 5 minutes. Also, higher bottom plenum back-pulse pressure will be used to account for the 55-to-36 filter element ratio on the bottom and top plenums.

Hopefully, the changes made during this outage, such as removing the 2-meter filter elements and tie wires, will prevent g-ash bridging during TC07; however, if the g-ash bridging occurs, then the addition of pressure and temperature measurements will produce some understanding behind the g-ash formation mechanism.

Upon inspection of the filter elements, the g-ash was noticed to be very fluffy. According to SRI this was the first time that they were able to take dustcake samples by simply brushing the samples off. In the past the g-ash has been very adherent to the filter elements. It is believed that in the past tar condensation in the PCD made the dustcake on the filter elements very sticky. [Figure 3.3-18](#) shows the filter elements after they were cleaned off with an air cannon. In the past the only method to clean the filter elements with a dustcake that was very adherent was pressure washing. It appears that the addition of the coke breeze feeder helped reduce tar, which resulted in this less adherent g-ash. See Section 3.4 for more details concerning dustcake properties.

[Figure 3.3-19](#) shows a large amount of g-ash buildup on the filter element on the lower plenum. [Figure 3.3-20](#) shows very little g-ash buildup on the lower support brackets. The g-ash buildup on the top plenum was relatively small. [Figures 3.3-21](#) and [-22](#) show the accumulated g-ash on the top and bottom ash shed, respectively. [Figure 3.3-23](#) shows that there was very little g-ash buildup on the inside wall of the shroud. Also, there was very little buildup on the liner sections.

The clean side of the tubesheet appeared to be in good condition. [Figure 3.3-24](#) shows that there was very little g-ash penetration to the insulation on the clean side of the tubesheet. [Figure 3.3-25](#) shows the condition of the insulation of the PCD head.

3.3.3.2 TC06B Filter Elements

[Figure 3.3-26](#) shows the filter layout for TC06B. Upon initial inspection all the filters appeared to be intact and undamaged; however, there was a considerable amount of g-ash bridging. Once the upper and lower plenums were cleaned each filter element was visually inspected.

During TC06B, 40 Pall 1.5-meter Fe₃Al filter elements; 38 Pall 1.5-meter Fe₃Al filters with fuse; 4 Pall 2-meter Fe₃Al filters with no fuse; and 2 Pall 2-meter Fe₃Al filters with fuse were used. The filter elements were visually inspected and no obvious damage was found. During this outage, 37 Pall Fe₃Al filters were removed. All filter elements were considered clean on the inside, which means that no loose g-ash was found inside any of the elements. After TC06B some of the Fe₃Al filters had accumulated 1,450 on-coal hours. Four of the Fe₃Al filters that were removed were sent to SRI for material testing. Test results from these elements will be provided in the TC07 run report.

During TC06B, four Pall 1.5-meter Hastelloy X filters were tested. The filter elements were visually inspected and no obvious damage was found. During this outage, two Pall 1.5-meter Hastelloy X filters were removed. All the filter elements were considered to be clean on the inside. After TC06B, 3 of the 4 Pall Hastelloy X filter elements had accumulated 1,025 on-coal hours.

During TC06B, two 1.5-meter U.S. Filter filter elements were tested. PSDF is currently working with U.S. Filter to test new filter element materials. Both filter elements were sintered metal fiber filters. The material of construction for one filter was Fecralloy-M. The materials of construction for the other filter were Haynes Alloys 214, 160, and 230. Each filter was visually inspected and no damage was noticed. Since this was the first time that either of these materials were tested at the PSDF, two Pall fuse safeguard devices were modified and installed above each filter. During the inspection each failsafe was removed and inspected. Each failsafe appeared to be clean, which indicated that the new filter elements did not leak. The materials of construction were chosen based on their corrosion resistance in reducing environments. Each of these filters was sent back to U.S. Filter for further testing to see if the materials had degraded or blinded. Based on their recommendations, further material testing will be pursued.

During this outage all of the bottom support brackets were removed to inspect the filters for bowing. Five of the 1.5-meter Fe₃Al filters bowed during TC06A as a result of the thermal incident. After the support brackets were removed no bowing was observed.

3.3.3.3 TC06B Filter Element Gaskets

During this outage 44 filter elements were removed and inspected. Also, 16 failsafe devices were removed and inspected. As each filter and failsafe device was inspected the filter element

gaskets were inspected as well. The gasket types are outlined in Section 3.3.2.3. Based on the inspection of these gaskets, the following observations were made:

- There were no leak paths in the area of the failsafe holder flanges that would indicate a leak past the sealing gasket.
- Some of the gaskets were cut to inspect the extent of the g-ash penetration. The inside of the sealing gaskets were relatively clean.
- The gaskets between the failsafe and plenum were clean.

The gasket material performed well throughout the 1,025 on-coal hours. This is based on the fact that the outlet loading was below 1 ppmw.

3.3.3.4 TC06B Failsafes

During TC06B four different types of failsafe devices were tested. These failsafe devices included:

- Standard Siemens Westinghouse failsafe device.
- New prototype Siemens Westinghouse failsafe device.
- Pall fuse.
- PSDF-designed failsafe device.

During this outage 16 failsafe devices and 17 Pall Fe₃Al filters with fuses were removed and inspected.

One standard Siemens Westinghouse failsafe device was removed. It was inspected and no evidence of damage was observed. Also, several filter elements that were below the standard failsafe design were removed and from that perspective the failsafe devices appeared to be in good condition.

During this outage nine of the new prototype Siemens Westinghouse failsafe devices containing metal fiber made from a variety of alloys were removed. These failsafe devices were weighed and flow tested. All of the failsafe devices, with the exception of one, weighed between 0.1 to 0.3 grams less than they did after GCT2. The other failsafe weighed 2.3 grams less than after GCT2. All the failsafe devices, with the exception of one, had flow coefficients that were lower than the flow coefficients that were measured after GCT2 by 1 to 6 percent. The reduction in flow coefficients was thought to be due to settling of the fiber rather than fouling. These failsafe devices will be installed for further testing. The failsafe device that weighed 2.3 grams less had a flow coefficient that was 5 percent higher than that measured after GCT2. It appears that the failsafe has lost some material. This failsafe device will not be installed in the next run.

The Pall Fe₃Al filters that were removed and had a fuse were inspected. All the fuses appeared to be in good condition and intact. Inspection of the filtering side of the fuse is not possible without destroying the filter, so conclusive comments with respect to the fuses are not possible at this time.

Before TC06A, four PSDF-designed failsafe devices were installed for syngas exposure testing. The purpose of this initial test was to determine whether or not this new design would be able to handle the severe conditions of gasification environment and back-pulse events while maintaining its mechanical integrity. After TC06B, the PSDF-designed failsafe devices were removed and inspected and appeared to be in good condition with no evidence of failsafe corrosion or damage. Based on these initial test results, further testing on these failsafe devices will continue.

3.3.3.5 TC06B Auxiliary Equipment

The filter element surface thermocouples that were also used during TC06A were used during TC06B. During this outage the thermocouples were inspected and no damage was noticed. The thermocouples were installed on individual filters to monitor the local temperatures. It is believed that the thermocouples will play a key role in determining the mechanism of g-ash formation; therefore, 26 thermocouples will be installed prior to TC07.

The back-pulse pipes were removed and inspected during this outage. Inspection of the back-pulse pipes didn't reveal any significant damage. There was no significant tar buildup on the pulse pipes and the inner liner appeared to be in good condition. [Figure 3.3-27](#) shows the condition of the back-pulse pipes after TC06B.

During the outage it was noticed that the two 4-inch carbon steel pipe studs that the pulse pipes pass through on the PCD head were badly corroded. In the past, scale has been reported on top of the failsafes; therefore, the pipe studs were replaced with 310 stainless steel during this outage. The lengths of the new pipe studs were adjusted using field measurements to maintain the specified gaps between the ends of the pulse pipes and the venturi inlets.

During the last two gasification test runs, the ball valves (SV3104A and SV3106B) upstream of the back-pulse valves (SV3111A and SV3112A) had problems closing when the back-pulse pressure was higher than 600 psid. During this outage the ball valves were replaced. The new valves should allow back-pulse testing at higher pressures during TC07.

3.3.3.6 TC06B Fine Solids Removal System Inspection

The fine solid removal system performed well during TC06. During the TC06B outage, the spent fines removal system was thoroughly inspected. The inspection included disassembling the screw cooler and the lock vessel system.

The screw cooler (FD0502) performed well during TC06 based on the fact that after 1,025 on-coal hours, FD0502 did not fail. Other than minor packing adjustments, the screw cooler required no maintenance. During the outage FD0502 was disassembled and inspected. A large

amount of g-ash was caked up in the screw cooler and in the drop pipe to the lock-vessel system. This cake was very wet and had the consistency of mud. The primary gas cooler had a leak in a couple of the tubes. It is believed that at the end of the run the steam being injected into the process through these leaks condensed once the temperature dropped during shut down. The condensation caused the g-ash to plug the screw cooler.

The packing rings appeared to be in good condition. Also, the stuffing box was inspected and no damage was noted (See [Figure 3.3-28](#)). The wear sleeve and shaft appeared to be in good condition as well (See [Figures 3.3-29 and -30](#)).

In an attempt to increase reliability, several modifications were made to the stuffing box during this outage. The lantern ring was increased to $\frac{3}{4}$ from $\frac{1}{2}$ in. to allow for more adjustment room. Also, the current stuffing box had the lantern ring positioned with five packing rings on each side of it. In order to add flow resistance and keep the purge gas toward the system instead of escaping to the atmosphere, the lantern ring was moved so that there were two packing rings between the lantern ring and the system. Therefore, eight packing rings were between the lantern rings and the outside of the system. Once again, this was done to promote purge gas flow in toward the system. Finally, the packing follower and guide studs were extended to allow more room to adjust the follower.

During this outage a Teflon plate was installed internally on the shaft of FD0502 on the outlet end. It is believed that as the drop-pipe between the screw cooler and the lock-vessel fills, solids are forced by the screw cooler into the packing, which ultimately contributes to failure. The Teflon plate was installed to act as a deflector and keep the solids out of the packing. It is believed that these modifications will keep the solids out of the packing and lead to increased reliability.

The lock-vessel (FD0520) system performed well during TC06B. There was one incident where solids carryover overloaded the lock-vessel system and caused the outlet pipe to plug. Since GCT1A, the FD0520 system has cycled over 49,000 times. During the inspection the drop pipe between the screw cooler and the lock vessel was plugged with the wet g-ash. [Figures 3.3-31 and -32](#) show how severe the solid packing was during the inspection. Once the solids were removed, the upper and lower spheri valves were inspected. The upper spheri valve appeared to be in good condition (See [Figure 3.3-33](#)). There was no scoring or sign of solid penetration past the dome valve. Also, the upper spheri valve inflatable seal was inspected and no visible damage was noticed (See [Figure 3.3-34](#)). The top ring plate was inspected and no damage was noted (See [Figure 3.3-35](#)). Next the lower spheri valve was inspected. The lower dome valve was in good condition and no damage was noted. The lower spheri valve inflatable seal was inspected and no sign of g-ash penetration was noted. The ring plate was inspected and no sign of damage was observed. Since all of the components appeared to be in good condition, they were reinstalled for TC07.

Table 3.3-1

TC06A PCD Operating Parameters

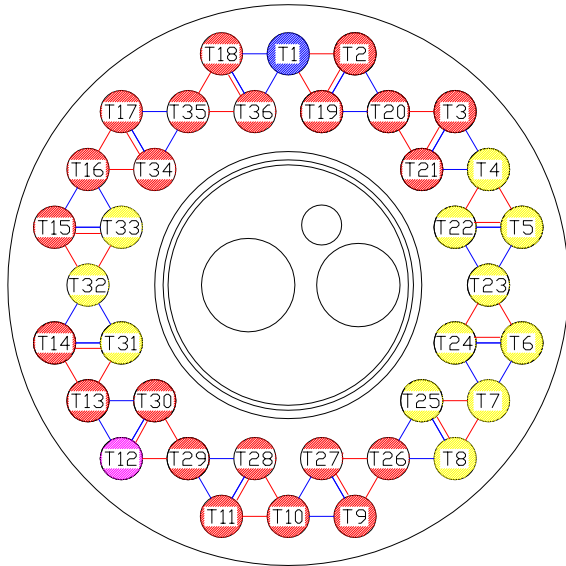
Element Layout	Layout 20 (Figure 3.3-1)
Filtration Area	261.3 ft ²
Back-pulse Pressure	200 to 400 psig Above Reactor Pressure (Approximate)
Back-pulse Timer	Set to 5 min (Varied Between 5 and 20 min)
Back-pulse High-Pressure Trigger Point	250 to 275 inH ₂ O
Back-pulse Valve-Open Time	0.2 sec
Inlet Gas Temperature	750 to 800°F (Approximate)
Face Velocity	3 to 4 ft/min (Approximate)
Baseline DP	80 to 140 inH ₂ O (Approximate)
Peak DP	140 to 270 inH ₂ O
Inlet Loading (SRI Sampling)	7,000 to 18,800 ppmw
Outlet Loading (SRI Sampling)	0.10 ppmw (During Normal Operation) and 22.9 ppmw (When Leaking Due to Filter Element Failure)
Coal/Sorbent	PRB/Dolomite

Table 3.3-2

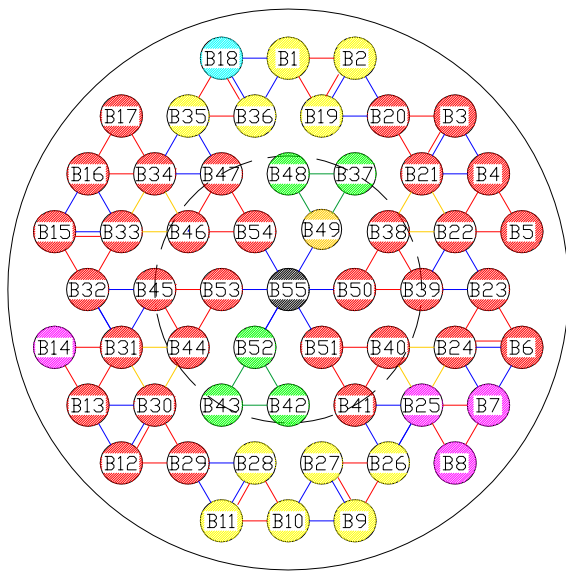
TC06B PCD Operating Parameters

Element Layout	Layout 21 (Figure 3.3-26)
Filtration Area	261.3 ft ²
Back-pulse Pressure	200 to 400 psig Above Reactor Pressure (Approximate)
Back-pulse Timer	Set to 5 min (Varied Between 5 and 20 min)
Back-pulse High-Pressure Trigger Point	250 – 275 inH ₂ O
Back-pulse Valve-Open Time	0.2 sec
Inlet Gas Temperature	670 to 750°F (Approximate)
Face Velocity	2.3 to 4 ft/min (Approximate)
Baseline DP	80 to 125 inH ₂ O (Approximate)
Peak DP	140 to 275 inH ₂ O
Inlet Loading (SRI Sampling)	9,300 to 17,000 ppmw
Outlet Loading (SRI Sampling)	< 0.1 ppmw
Coal/Sorbent	PRB/Dolomite

Layout 20 (TC06)
(A=261.3 ft²)



TOP PLENUM
(VIEWED FROM TOP)



BOTTOM PLENUM
(VIEWED FROM TOP)

- Pall FEAL-1.5m (54)
- Pall FEAL-1.5m/Fuse (23)
- Pall FEAL-2m (5)
- Pall FEAL-2m/Fuse (1)
- Pall Hastelloy X (5)
- USF Fecraloy /Pall Fuse (1)
- USF Haynes /Pall Fuse (1)
- Support Post (1)
- Support at Level 2
- Support at Level 3a
- Support at Level 3b
- Support at Level 3c
- Support at Level 4

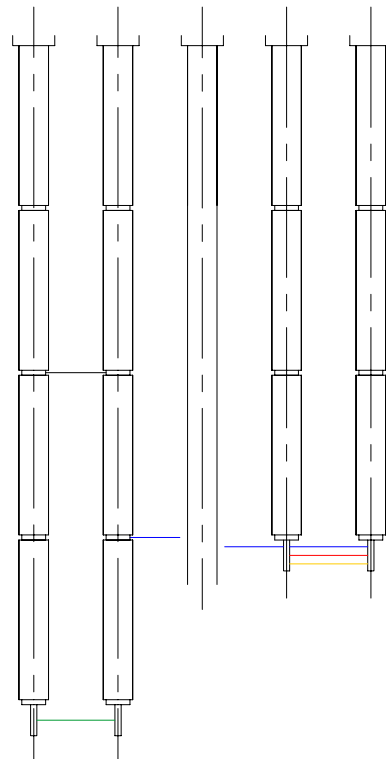


Figure 3.3-1 TC06A Tubesheet Layout

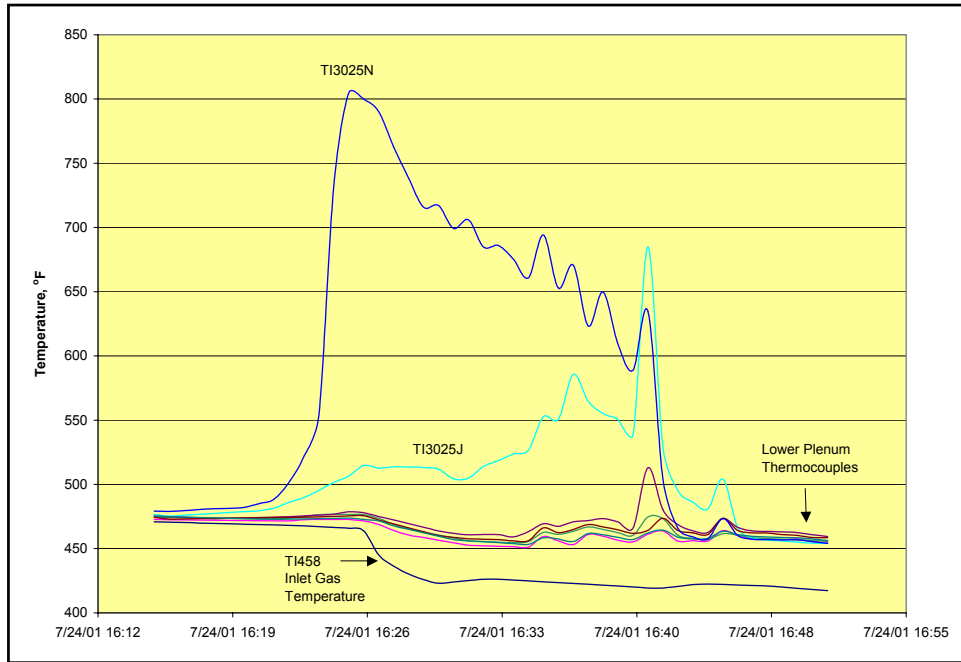


Figure 3.3-2 Temperature Excursion on the Lower Plenum

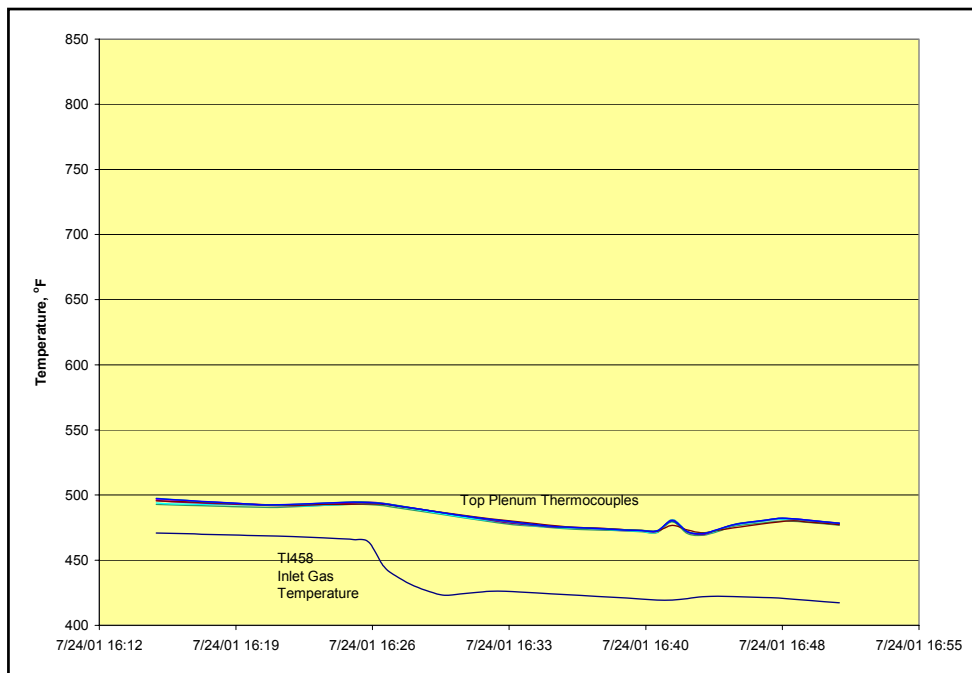


Figure 3.3-3 Top Plenum Response During the Temperature Excursion

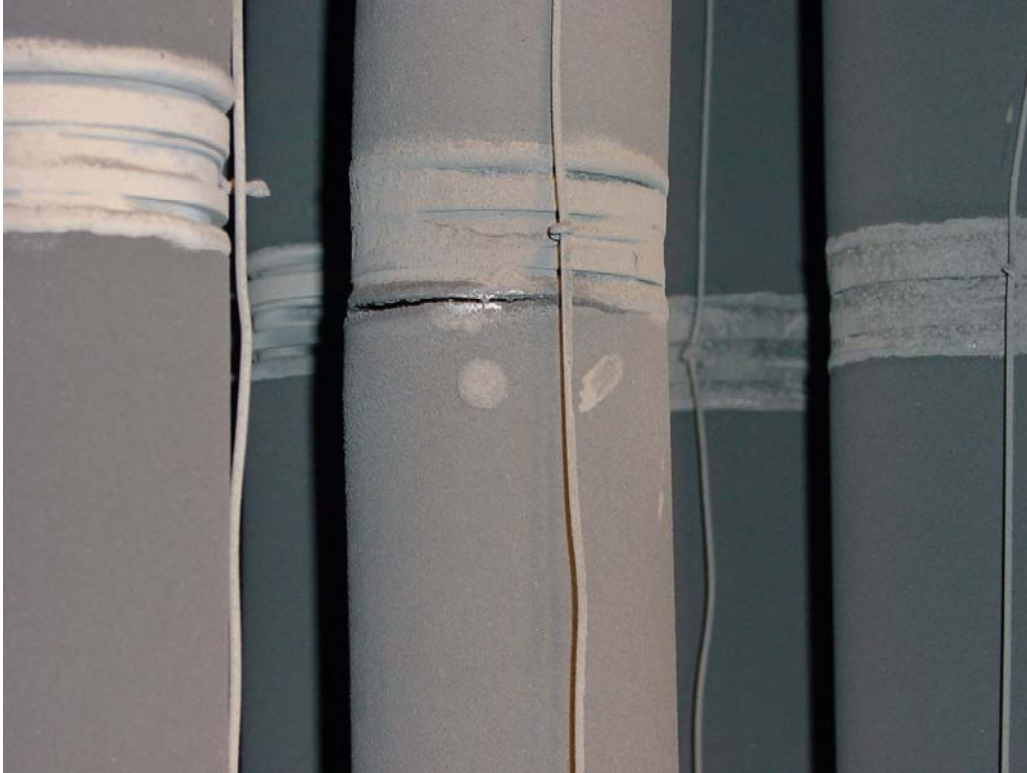


Figure 3.3-4 Failed Fe₃Al Filter (B-32)

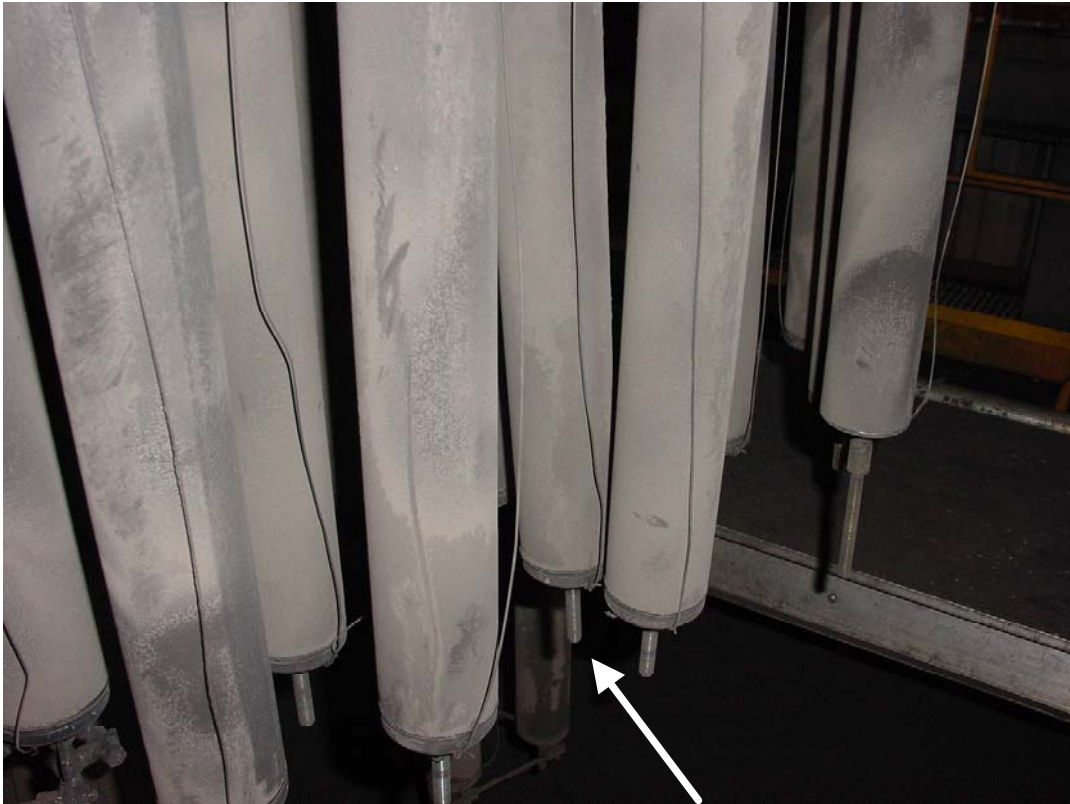
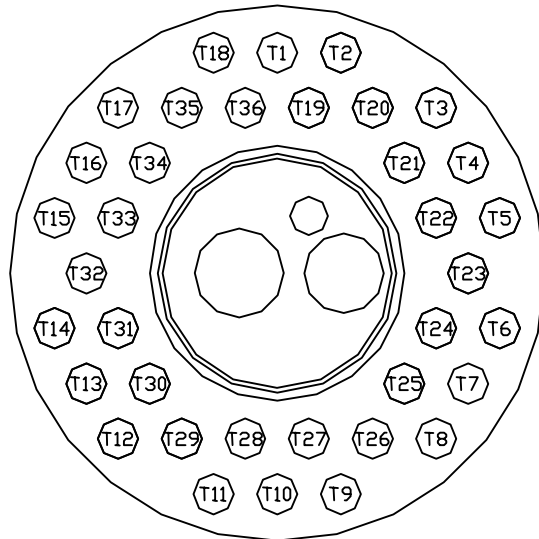





Figure 3.3-5 Bowed Fe₃Al Filters on Lower Plenum

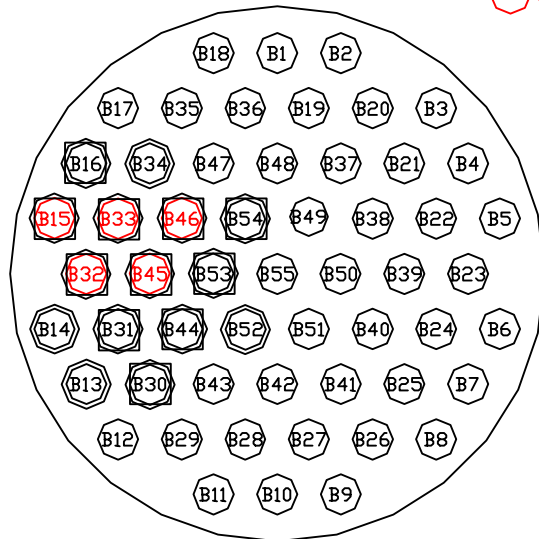
Layout 20 (TC06)
 (A=261.3 ft²)

NORTH



TOP PLENUM
 (VIEWED FROM TOP)

-  Removed Candles
-  Dirty Failsafes
-  Bowed and with Discolored Patches



BOTTOM PLENUM
 (VIEWED FROM TOP)

Figure 3.3-6 Filter Layout of Bowed Filters

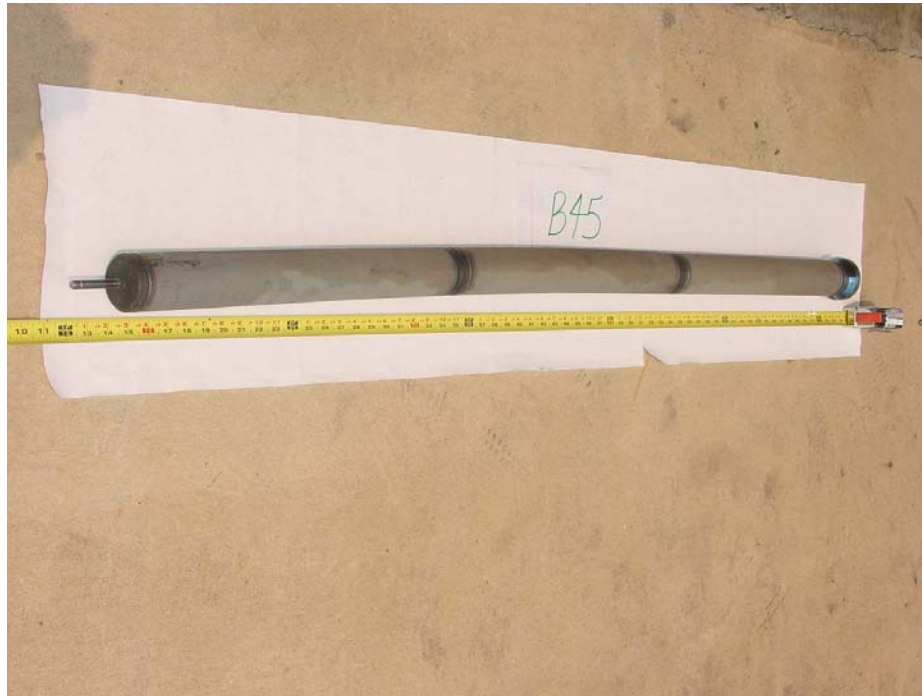


Figure 3.3-7 Abnormal Color Pattern After TC06A



Figure 3.3-8 Abnormal Color Pattern After TC06A

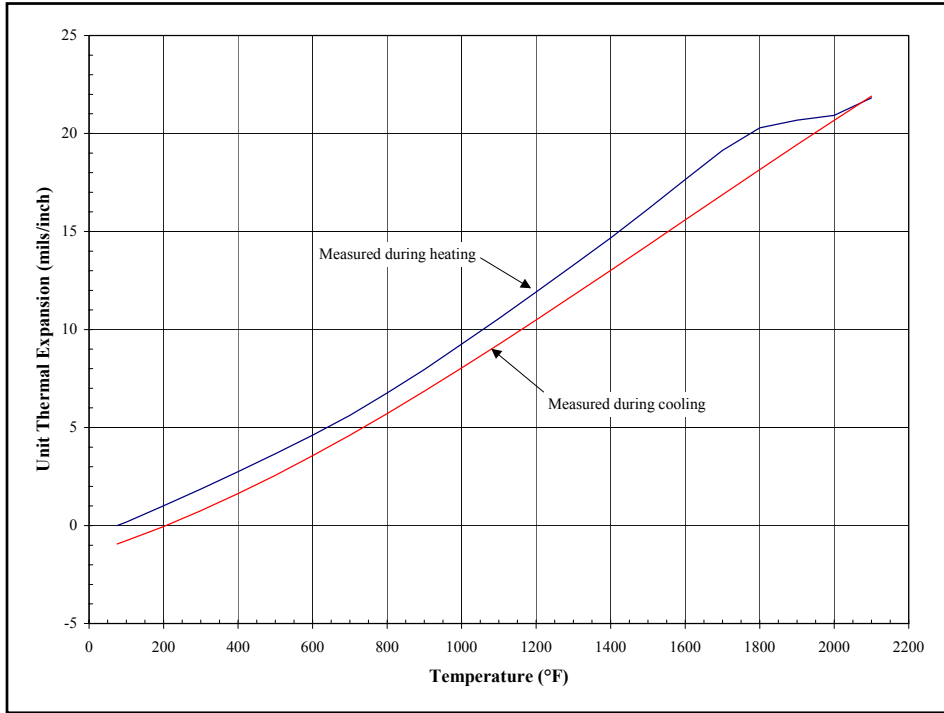


Figure 3.3-9 Thermal Expansion Test Results



Figure 3.3-10 PCD Internal Removal (Lower Plenum)



Figure 3.3-11 G-ash Accumulation on Top Ash Shed



Figure 3.3-12 PCD Internal Shroud and Liner



Figure 3.3-13 Tubesheet Insulation



Figure 3.3-14 Insulation in the Head of the PCD



Figure 3.3-15 Removal of PCD Internals After TC06B

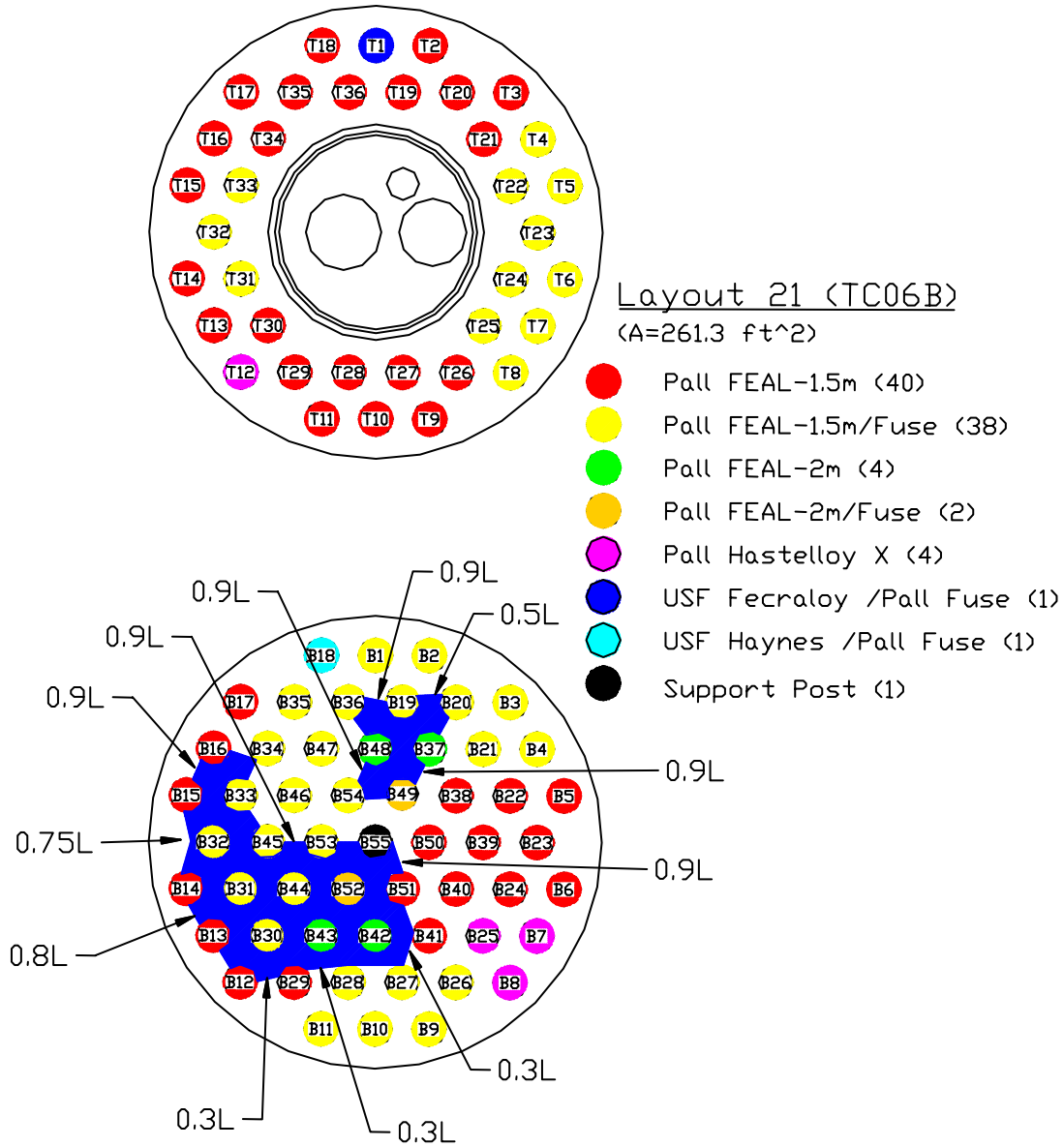


Figure 3.3-16 Location of G-ash Bridging After TC06B



Figure 3.3-17 G-ash Bridging Over TI3025J



Figure 3.3-18 Filters After Being Cleaned With Air



Figure 3.3-19 G-ash Buildup on Filter Element Fixtures

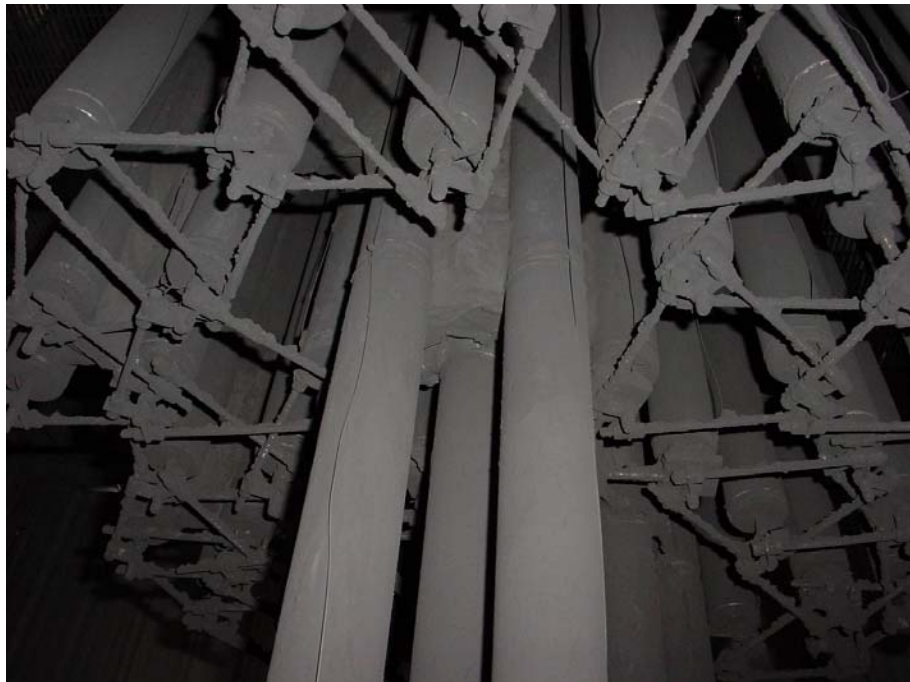


Figure 3.3-20 G-ash Buildup on Lower Support Brackets



Figure 3.3-21 G-ash Buildup on Top Ash Shed



Figure 3.3-22 G-ash Buildup on Bottom Ash Shed

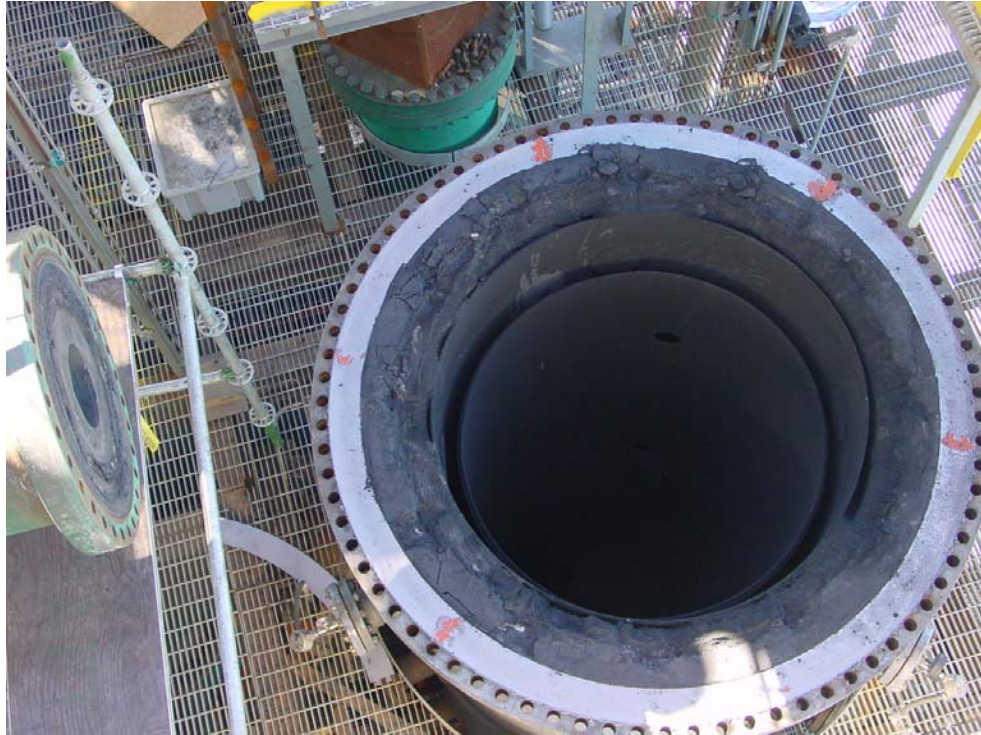


Figure 3.3-23 PCD Shroud and Liner



Figure 3.3-24 Tubesheet Insulation



Figure 3.3-25 PCD Head Insulation

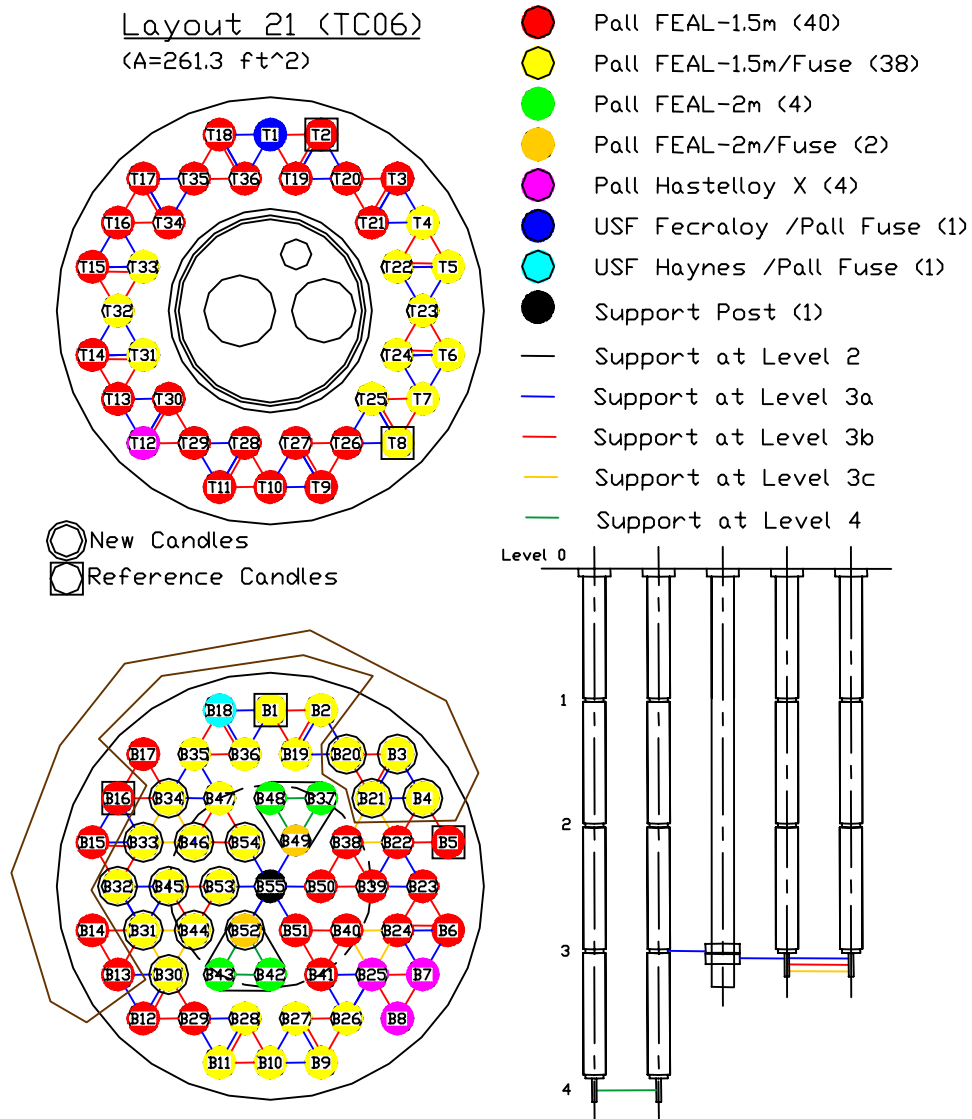


Figure 3.3-26 TC06B Filter Element Layout



Figure 3.3-27 Back-Pulse Pipes After TC06B

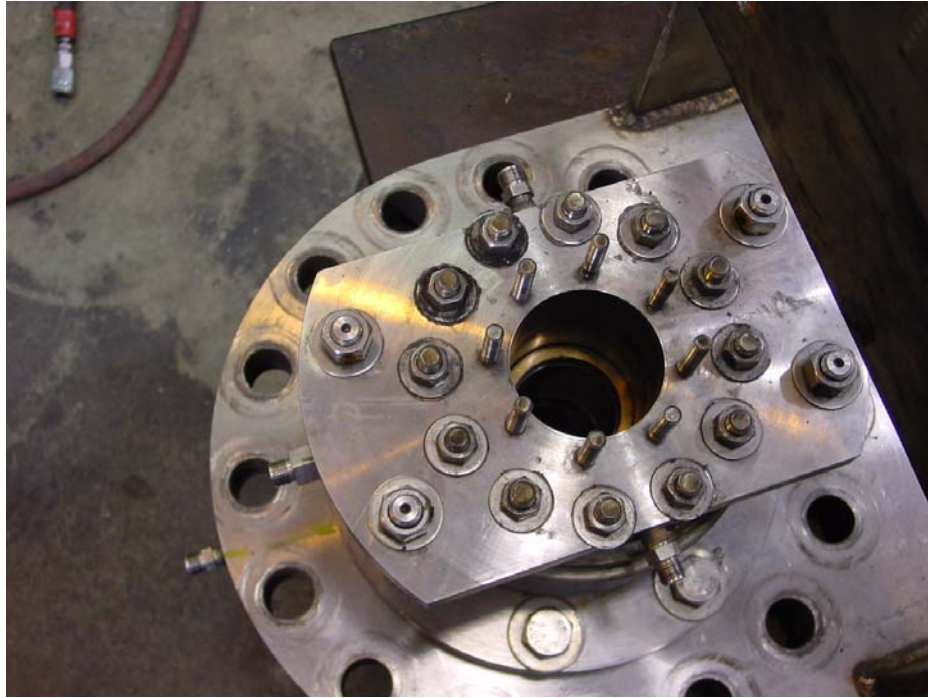


Figure 3.3-28 FD0502 Stuffing Box After TC06

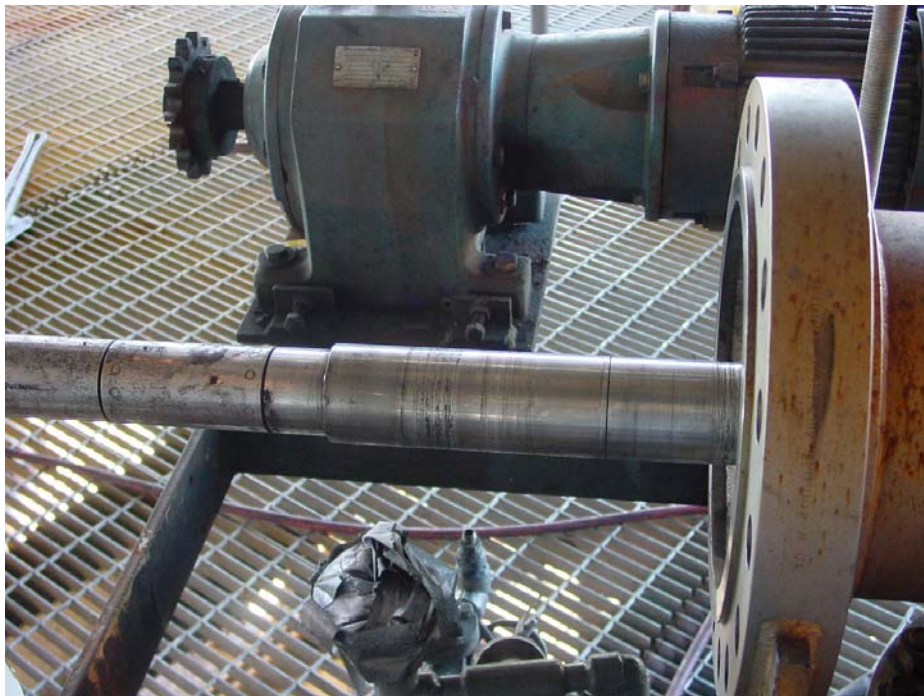


Figure 3.3-29 FD0502 Drive End Wear Sleeve and Shaft



Figure 3.3-30 FD0502 Nondrive End Wear Sleeve and Shaft



Figure 3.3-31 Drop Pipe Between FD0502 and FD0520



Figure 3.3-32 Upper Spheri Valve on FD0520



Figure 3.3-33 Upper Spheri Valve After Cleaning



Figure 3.3-34 Upper Spheri Valve Inflatable Seal After TC06

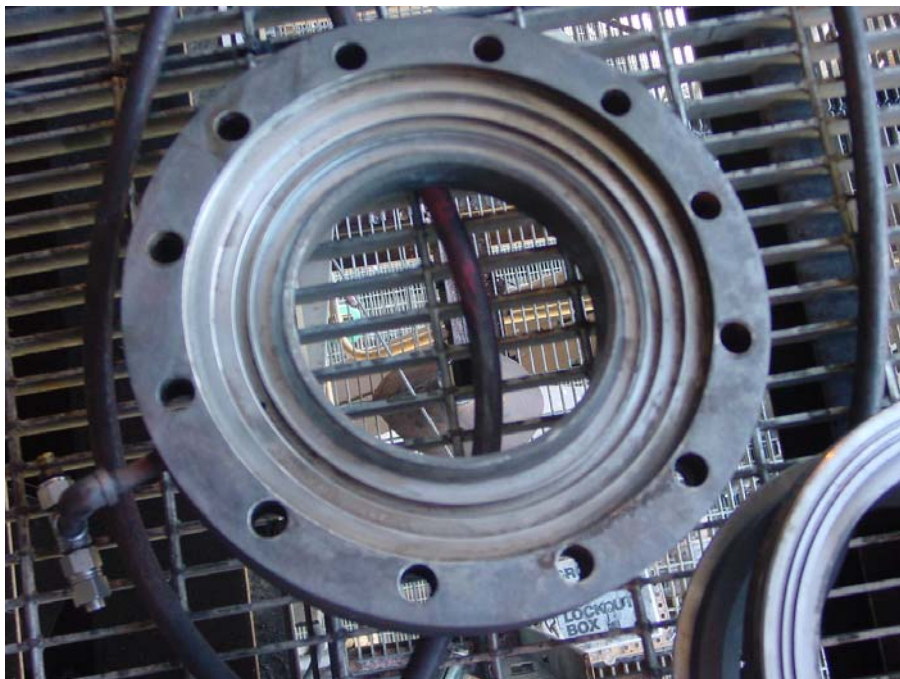


Figure 3.3-35 Top Ring Plate for FD0520 After TC06

3.4 TC06 GASIFICATION ASH (G-ASH) CHARACTERISTICS AND PCD PERFORMANCE

This section reports the characteristics of the g-ash produced during TC06 and the relationship between the g-ash characteristics and PCD performance. As in previous tests, in situ g-ash samples and dustcake samples from TC06 were thoroughly characterized in an effort to better understand the effects of the g-ash characteristics on filter pressure drop and the formation of bridged deposits. G-ash samples were collected at the PCD inlet and at the PCD outlet throughout TC06 using the SRI in situ sampling system described in previous reports. Dustcake samples were collected after both portions of the TC06 run (TC06A and TC06B) even though the samples collected after TC06A were not representative of normal operation as a result of the thermal transient that occurred in the PCD during tuning of the main air compressor. There were no such anomalies after TC06B, and representative samples of the residual dustcake, transient dustcake, and bridged deposits were obtained after that test segment. Characterization of the in situ g-ash samples, dustcake samples, and bridged deposits included: chemical analyses; particle-size analyses; laboratory drag measurements; and measurements of the true particle density, bulk density, uncompacted bulk porosity, and specific-surface area. As in the previous gasification tests, drag measurements were made using the resuspended ash permeability tester (RAPTOR) as modified to allow measurements as a function of particle size. As in previous tests, the RAPTOR drag measurements were compared to transient drag values determined from PCD performance data, and the results were used to gain a better understanding of the contribution of the dustcake to PCD ΔP and to gain insight into the effect of particle size and morphology on drag.

3.4.1 In situ Sampling

As in previous test campaigns, in situ particulate sampling runs were performed on a regular basis at the PCD inlet and the PCD outlet throughout TC06. The system and procedures used for the in situ particulate sampling have been described in previous reports. During TC06, a total of 27 particulate sampling runs were performed at the PCD inlet and 31 particulate sampling runs were performed at the PCD outlet.

3.4.1.1 PCD Inlet Particle Mass Concentrations

Table 3.4-1 is a summary of the particulate loadings measured at the PCD inlet during TC06. Excluding the two runs performed during coke feed (run Nos. 1 and 3) and the one run performed in the absence of limestone addition (run No. 4), the TC06 inlet mass loadings varied from 9,200 to 18,800 ppmw, with a mean value of 13,900 ppmw and a standard deviation of 2,900 ppmw (coefficient of variation of 0.21). The substantial variation in the inlet loading is largely attributable to the inclusion of eight runs that were performed during periods of low coal-feed rate. Excluding these runs (run Nos. 7, 12, 13, 21 through 24, and 26), the average inlet loading is increased to 15,700 ppmw with a standard deviation of 1,700 ppmw (coefficient of variation of 0.11). This average value is still somewhat lower than the average inlet loading measured during GCT3 and GCT4, which was 18,400 ppmw with a standard deviation of 6,000 ppmw (coefficient of variation of 0.33). Considering the variability of the measurements, however, the difference between the TC06 and the GCT3/GCT4 mass loadings is not statistically significant. The TC06 and GCT3/GCT4 mass loadings are, however, significantly different from those measured in GCT2, in which the mean mass loading was 31,100 ppmw

with a standard deviation of 2,600 ppmw (coefficient of variation of 0.08). This difference reflects the changes made in the Transport Reactor recycle loop between GCT2 and GCT3.

The inlet mass concentration measured during startup on coke breeze is shown by run Nos. 1 and 3. These data indicate that the PCD inlet particulate concentration during coke operation was approximately one-half the average of that obtained during coal operation. This is consistent with PCD operational data, which indicated that PCD ΔP was very low during coke startup.

3.4.1.2 PCD Outlet Particle Mass Concentrations

Table 3.4-1 shows the particle concentrations measured at the outlet of the PCD along with the PCD collection efficiency calculated from the corresponding inlet and outlet mass measurements. Except for one sampling run performed at the end of TC06A (outlet sample No. 8 in Table 3.4-1), the PCD operated with very low outlet loadings, consistent with an absence of significant leaks. The high loading for outlet sample No. 8 was obtained after the PCD thermal transient, which resulted in a cracked filter element as discussed in the section on PCD operations (see Section 3.2). Excluding this run and the runs performed during particulate monitor calibration (discussed in a later section), the outlet loading was always below the lower limit of resolution of the measurement with an average collection efficiency exceeding 99.997 percent. As indicated in the table, the lower limit of resolution of these particulate measurements varied from 0.1 to 0.4 ppmw depending on the test duration.

3.4.1.3 Tar Contamination

In previous gasification runs, particulate samples have sometimes shown evidence of tar contamination. Evidence of tar formation has also been seen in the form of sticky residual dustcakes and condensed tar components found in the gas analysis system. The tar was apparently formed when coal was introduced into the Transport Reactor system while the temperatures in the system were too low to completely crack the tar components. To address this problem, a system for feeding coke breeze was added prior to TC06. This system makes it possible to heat the Transport Reactor system to the temperatures required for tar cracking before coal is introduced. With the coke feed system in use, the TC06 particulate samples showed no evidence of tar contamination.

3.4.1.4 Syngas Moisture Content

As in previous tests, measurements of the syngas moisture content were made in conjunction with the outlet particulate sampling runs. The water vapor content of the syngas was determined by collecting the condensate from the syngas in an ice-bath condenser and calculating the vapor concentration from the volume of gas sampled and the volume of condensate collected. The values determined for individual runs are included in Table 3.4-1. Based on these data, the TC06 syngas moisture content varied from 4.6 to 10.9 percent, with a mean value of 7.6 percent and a standard deviation of 1.3 percent (coefficient of variation of 0.17). In the section on Transport Reactor operations, these measurements are compared to moisture data obtained from on-line instrumentation. Much of the variation in syngas moisture content is a result of changes in steam-injection rates.

3.4.2 PCD Dustcakes and Consolidated Deposits

Following both segments of TC06, samples were collected of the dustcakes and any bridged deposits that remained in the PCD. After TC06A, there was only a very thin residual dustcake remaining in the PCD, and the dustcake may not have been representative of normal operation as a result of the thermal transient that occurred at the end of TC06A, resulting in a cracked filter element. Chemical analysis suggests that the TC06A residual cake was partially combusted during the thermal transient. No transient dustcake and no bridged deposits were present in the PCD after TC06A.

At the conclusion of TC06B, a dirty shutdown of the PCD was performed to allow sampling of both residual and transient dustcakes as well as any bridged deposits that may have been present. Even though a dirty shutdown was performed, there were areas of the filter surfaces that were completely devoid of dustcake. Other areas were covered with what appeared to be the residual dustcake and there were several patches of what appeared to be transient dustcake. Most of the transient dustcake apparently fell off the filter elements before or during the removal of the filter internals. The remaining residual and transient dustcakes could be easily removed with a soft-bristle brush and there was no evidence of any type of stickiness or consolidation in the dustcakes. This observation suggests that the TC06B dustcakes were not substantially affected by tar deposition as the GCT4 dustcakes were.

The TC06B residual cake was extremely thin (~0.01 in. average thickness). The thickness of the transient cake varied from about 0.09 to 0.15 in. Since there were only a few patches of transient cake remaining, and since some of the residual cake had apparently fallen off also, these thickness measurements are probably not reliable for any analysis of PCD ΔP . The patches of remaining dustcake were deemed to be too small and too irregular to make reliable measurements of the areal loadings, but the thicknesses of the cakes were estimated from measurements made within the small remaining patches. The dustcake areal loadings were then estimated from the thickness measurements, assuming that the porosity of the TC06 dustcake was the same as the porosity measured for the GCT3/GCT4 dustcakes (83 percent). Based on this assumption, the areal loadings of the TC06 residual and transient dustcakes were estimated to be 0.02 and 0.2 lb/ft², respectively. Again, these values of areal loading are probably not reliable since much of the transient cake and perhaps some of the residual cake had fallen off prior to the thickness measurements. The information below compares the average dustcake thicknesses and areal loadings for TC06B and GCT4 based on the assumption that the TC06 dustcake porosity was the same as the GCT4 dustcake porosity (83 percent).

	<u>Residual Dustcake</u>		<u>Transient Dustcake</u>	
	<u>TC06</u>	<u>GCT4</u>	<u>TC06</u>	<u>GCT4</u>
Thickness (in.)	0.01	0.1	0.12	0.3
Areal Loading (lb/ft ²)	0.02	0.2	0.24	0.6

As discussed previously, the thickness and areal loading values for TC06 are probably too low since some of the cake appeared to have fallen off prior to the thickness measurements. On the other hand, the thickness and areal loading values for GCT4 may be too high as a result of tar

deposition. The “appropriate” values of thickness and areal loading probably lie between the TC06 and GCT4 values given in the table above. Later in this report, the dustcake areal loadings will be estimated from dustcake drag measurements and data on PCD ΔP . Because of the uncertainties in the thickness measurements it is believed that the areal loadings that are estimated from the dustcake drag and the filter ΔP are more reliable than the values given above.

As discussed in the section on PCD inspection, bridged deposits were present between some of the filter elements in the bottom plenum after TC06B. There was no bridging in the top cluster. Roughly 25 percent of the filter surface in the bottom plenum appeared to be covered by the bridged deposits. The bridged g-ash appeared to be packed between the elements but it did not appear to be consolidated. It was impossible to remove intact chunks of the bridged material without the chunks breaking apart into loose dust. This observation suggests that the bridged material was not bonded together by tar or any other chemical consolidation mechanism.

To investigate the differences between the residual and transient cakes and the bridged material, all three types of samples were thoroughly characterized. In previous tests this characterization has included evaluation of both physical properties and chemical analysis but the analytical results have not been particularly useful in the evaluation of PCD performance. Therefore, this report will focus on the physical properties of the samples.

3.4.3 Physical Properties of In situ Samples and Dustcakes

The TC06 in situ particulate samples and dustcake samples were subjected to the standard suite of physical measurements, including true (skeletal) particle density, bulk density, uncompacted bulk porosity, specific-surface area, and particle-size analysis. The instruments and procedures used for making these measurements have been described in previous reports.

3.4.3.1 In situ Particulate Samples

Physical properties of the in situ particulate samples from TC06 are presented in detail in [Table 3.4-2](#), and the information listed below compares the average in situ physical properties for TC06 and GCT4.

	<u>TC06</u>	<u>GCT4</u>
Bulk density (g/cc)	0.29	0.27
Skeletal particle density (g/cc)	2.45	2.29
Uncompacted bulk porosity (%)	88.3	88.2
Specific surface area (m ² /g)	222	197
Mass-median diameter (μm)	15.3	15.9

Based on the above comparison, the g-ash produced in TC06 appears to be very similar to the g-ash produced in GCT4. Although the bulk density and true density of the TC06 g-ash are slightly higher than those of the GCT4 g-ash, the difference is small (about 7 percent), and in both cases the densities yield the same value of bulk porosity (88.3 percent). The differences in

surface area and mass-median diameter (MMD) are insignificant considering the variability of the data. The similarity of the TC06 and GCT4 g-ash is not surprising, since both were produced from the same Powder River Basin (PRB) coal and the same Ohio (bucyrus) limestone, and the operating conditions of the Transport Reactor system did not differ dramatically between GCT4 and TC06. The role of these physical properties in determining dustcake drag will be discussed in more detail in the section on drag measurements. A more detailed comparison of the TC06 and GCT4 particle-size distributions will be presented in the next section of this report.

Also included in [Table 3.4-2](#) are the physical properties of in situ samples collected during coke breeze startup (inlet runs 1 and 3). The coke samples have much lower values of specific surface area than do the samples obtained during coal operation. Consistent with PCD operational data, there does not appear to be any evidence that startup with coke should negatively affect PCD operation.

3.4.3.2 Dustcake Samples

The physical properties of the residual and transient dustcake samples and bridged deposits from TC06B are compiled in [Table 3.4-3](#), and the average properties of the various TC06B samples are compared to those from GCT4 in the listing below.

	Residual Dustcake		Transient Dustcake		Bridged G-ash	
	<u>TC06</u>	<u>GCT4</u>	<u>TC06</u>	<u>GCT4</u>	<u>TC06</u>	<u>GCT4</u>
Bulk density (g/cc)	0.25	0.34	0.25	-----	0.27	0.34
Skeletal particle density (g/cc)	2.28	1.91	2.39	-----	2.41	2.21
Uncompacted bulk porosity (%)	89.0	82.2	89.5	-----	88.8	84.6
Specific surface area (m ² /g)	257	8.0	261	-----	261	173
Mass-median diameter (μm)	9.3	8.4	9.2	-----	10.8	12.7

The properties of the GCT4 transient dustcake are not included in the comparison above because these samples were not representative of normal GCT4 operations as discussed in the GCT4 report. In comparing the residual dustcakes and bridged deposits it is apparent that both types of samples from TC06 have lower bulk densities, higher true (skeletal) particle densities, higher bulk porosities, and higher surface areas than do the GCT4 dustcakes and bridged deposits. These differences in the residual dustcakes and bridged deposits are interesting because there was very little difference between the TC06 and GCT4 in situ samples. One difference between the in situ samples and the other types of samples is that the in situ sampling avoids periods of tar formation, while the residual dustcakes and bridged deposits are unavoidably exposed to any tar deposition that may occur. This result suggests that the TC06 and GCT4 g-ashes are similar in the absence of tar formation and that the observed differences in the residual dustcakes and bridged deposits may be related to the tar deposition that occurred during GCT4.

3.4.4 Particle-Size Analysis of In situ Samples and Dustcakes

The average particle-size distribution of in situ dust samples entering the PCD during TC06 coal operation is shown in [Figure 3.4-1](#). Also shown on the figure is the average distribution from GCT4. The two distributions are nearly identical and show that no significant changes in particle size occurred between the two test programs. At least with PRB coal, Transport Reactor operation appears to have reached a stable, reproducible condition.

Startup and restart following lost coal feed during TC06 were conducted using coke breeze to reduce tar formation. The particle-size distribution measured at the PCD inlet during coke operation is compared to coal operation in [Figure 3.4-2](#). As shown in Section 3.4.1.1, the coke produced less overall mass than the coal. Comparison of the size distribution data indicates that the reduction occurred over almost the entire size range covered by the measurements. The coke data are largely unremarkable and there is no suggestion from the particle-size data that any operational problems would be expected because of coke operation.

The size distributions of samples removed from inside the PCD after shutdown are shown in [Figure 3.4-3](#). The solid symbols represent PCD dustcake samples while open symbols are the PCD inlet data discussed above. (The PCD dustcake samples shown here are only from TC06B because the dustcake samples of TC06A were damaged by the thermal transient at the end of the run.) The three dustcake samples (residual, transient, and bridged deposit) show almost exactly the same size distributions. This is different from previous test programs, which frequently indicated that the residual dustcake was finer than the transient dustcake or bridged deposits. The similarity of dustcakes may be attributable to the lack of tar formation during TC06, which resulted in residual dustcakes that were fluffy with low cohesivity. Unlike previous test programs, the TC06 residual dustcake was very thin and easily removed. Since the residual dustcake could be pulse cleaned more readily, there may have been less opportunity for fine-particle enrichment of a long-lived, residual dustcake that persisted throughout the run.

Comparison of the in situ and dustcake samples in [Figure 3.4-3](#) shows that the in situ distribution contained more large particles than were found in the dustcakes although the differences are minor. This difference could indicate some cyclonic separation of large particles by the tangential entry system, although evidence of this effect has been inconsistent over a number of test programs.

3.4.5 Laboratory Drag Characteristics of G-ash

At the end of TC06B, a dirty shutdown was attempted to preserve the transient dustcake in the PCD. While a quick and uneventful shutdown was successfully accomplished, very little transient dustcake remained by the time the PCD was disassembled. The g-ash was very fluffy and loose, with low cohesivity. Most of the transient dust simply fell off the filter elements and apparently took most of the residual dustcake with it (as discussed previously). The result was that insufficient material was recovered of either dustcake for laboratory drag measurements using the RAPTOR system. Only the bridged deposit was available in sufficient quantity for RAPTOR measurements. Therefore, for this analysis, both CAPTOR and RAPTOR data will be used to understand the dustcake drag characteristics from TC06. The CAPTOR will be used

to compare the three PCD samples (transient, residual, and bridged deposit), while the RAPTOR measurements will be made only on the bridged deposit.

CAPTOR drag, as a function of porosity for the three TC06B samples are shown in [Figure 3.4-4](#). Although there are some differences, the three curves are very similar. The solid symbols on the graph indicate the drag at the flow-compacted porosity (FCP) as determined from the CAPTOR measurement. The drag values at FCP ranged from 74 to 105 inWC/(ft/min)/(lb/ft²), which is a typical degree of scatter for this type of data.

For comparison with the TC06 data, CAPTOR data from dustcake samples collected in GCT2 and GCT4 are shown in [Figure 3.4-5](#). These drag curves show a substantial difference between the two GCT4 dustcakes with the transient drag comparable to the TC06 data and the tar-contaminated residual dustcake in a much lower drag range. Interestingly, the GCT2 transient and residual dustcakes are not very different despite the residual layer being contaminated with tar, with both indicating low drag. These data appear to suggest that tar contamination of a low-surface-area particulate, such as the GCT2 g-ash, does not have a significant effect on dustcake drag, while coating the high-surface-area particles from GCT4 with tar has a substantial effect on drag. This would seem to support the conclusion that the residual dustcake from TC06 was relatively free of tar and that the use of coke breeze during startup was effective in preventing residual dustcake contamination.

[Figure 3.4-6](#) shows the results of RAPTOR measurements of drag as a function of particle size for the TC06 bridged deposit sample. The solid circles represent the TC06 data, while the solid line is a regression fit to those data ($r^2 = 0.96$). For comparison, the regression fits to the GCT2 and GCT3/GCT4 data are also shown on the figure. The TC06 data are in substantial agreement with the other data collected since the modification of the Transport Reactor recycle loop (after GCT2). The agreement of the CAPTOR data for the residual and transient dustcake samples suggests that the RAPTOR data from the bridged deposit can be reasonably applied to all of the TC06 dustcakes.

In [Figure 3.4-7](#), specific surface areas measured on the RAPTOR samples are plotted as a function of the MMD of the sample. Also included on the graph are GCT2 and GCT4 data for comparison. In the GCT4 report, it was suggested that the large increase in surface area from GCT2 to GCT4 was caused by improved gasification and a resulting change in particle morphology. The relationships between surface area and MMD and between drag and MMD suggest that, at a given particle size, there is a definite effect of surface area on drag. However, the GCT4 hopper samples and bridged dustcake samples had similar drag characteristics despite the difference in surface area shown in [Figure 3.4-7](#). This difference in surface area was attributed to the deposition of tar in features too small to affect drag (submicron pores). The TC06 bridged deposit has both high surface area and high drag, despite what is presumed to be long exposure inside the PCD. This is another measure of the success of coke breeze startup in eliminating tar.

3.4.6 Analysis of PCD Pressure Drop

In this section, the contributions of the transient and residual dustcakes to PCD ΔP are examined by comparing dustcake drag values calculated from the PCD ΔP to dustcake drag values measured by RAPTOR. This is a very valuable comparison because mismatches between these two methods of determining drag can indicate that other factors (i.e., tar deposition) may be influencing the PCD ΔP .

3.4.6.1 PCD Transient ΔP Analysis

This analysis was done using the same procedure described in detail in the GCT3 and GCT4 reports. For each in situ particulate sampling run, the transient PCD drag during the run was determined from the rate of ΔP rise during the run and the rate of g-ash accumulation in the transient cake. The latter was determined from the measured particulate loading and the syngas mass-flow rate during the run. To allow direct comparison of this PCD drag value with the RAPTOR drag measurements, the PCD drag was adjusted to the RAPTOR conditions using the ratio of the syngas viscosity at process temperature to the viscosity of air at laboratory room temperature. The RAPTOR drag value for each particulate sampling run was taken from the plot of drag versus MMD shown previously in [Figure 3.4-6](#) using the MMD values determined by Microtrac analysis for each sampling run.

[Table 3.4-4](#) summarizes the PCD transient drag calculations discussed above and compares the PCD transient drag values to the corresponding drag values measured by RAPTOR. As in the previous data analysis, the sampling runs performed during coke feed and during low coal feed have been excluded. Average values of PCD transient drag and RAPTOR drag are given below for both TC06 and GCT4. The drag values are on the viscosity basis of air at 77°F.

	<u>TC06</u>	<u>GCT4</u>
Average Drag from PCD $\Delta P/\Delta t$ (inWC/(lb/ft ²)/(ft/min))	83	66
Average Drag from RAPTOR Data (inWC/(lb/ft ²)/(ft/min))	94	70

This summary shows that there is good agreement between the PCD performance calculations and the RAPTOR measurements. This agreement can also be seen by plotting the individual values of PCD drag and RAPTOR drag determined for each sampling run, as shown in [Figure 3.4-8](#). This plot shows that the RAPTOR drag values track the PCD transient drag values reasonably well. This result suggests that the flow resistance of the g-ash is high enough to account for all of the transient ΔP , and that the transient dustcake drag was not affected by tar deposition or other anomalies during the in situ particulate sampling runs.

Laboratory measurements of drag were also made with a sample collected during startup on coke breeze. The normalized drag at CAPTOR FCP was determined to be 23 inWC/(lb/ft²)/(ft/min) on PCD inlet in situ run No. 3. This drag is much lower than the average value obtained for coal operation [94 inWC/(lb/ft²)/(ft/min)]. The actual PCD drag (corrected to room temperature) during the period of the in situ test was 17 inWC/(lb/ft²)/

(ft/min), which is in good agreement with the lab measurement. Thus, both the calculated transient PCD drag and the laboratory-measured drag suggest that PCD performance should not have been adversely affected by using coke breeze as the start-up fuel.

3.4.6.2 PCD Baseline ΔP Analysis

In the section on PCD operations analysis, a plot is shown of the normalized baseline ΔP as a function of time throughout TC06. As shown in the plot, the normalized baseline ΔP remained fairly stable at around 80 inWC until about September 2, 2001. At that point, the normalized baseline ΔP slowly increased, reaching a maximum value of about 100 inWC after about 10 days. Tar deposition does not appear to have been a major contributing factor in the increasing baseline ΔP , since the residual dustcake was easily removed and did not appear to be bonded together with tar. In the absence of tar-related effects on the residual dustcake, the most likely cause of the increasing baseline ΔP is the formation of bridged deposits. In order to separate the effect of the residual dustcake ΔP from the effect of the bridged deposits, the analysis of baseline ΔP will be done using the stable baseline ΔP value (80 inWC) that was recorded prior to the suspected bridging.

As shown in previous reports, the contribution of the residual dustcake to the baseline ΔP can be estimated by subtracting out the contributions of the vessel losses and any irreversible increases in the filter element ΔP and the failsafe ΔP . Vessel losses and irreversible changes in filter element and failsafe ΔP , normalized to the same conditions as the baseline ΔP , were estimated to be 30 and 3 inWC, respectively. After subtracting out these contributions, the remaining normalized ΔP that can be attributed to the residual dustcake is 47 inWC. To allow direct comparison with the laboratory drag measurements, this value of residual dustcake ΔP must be corrected to the same viscosity basis as the RAPTOR measurements (air at room temperature). In this case, the corrected residual dustcake ΔP value at room temperature is 29 inWC.

Since some of the residual dustcake apparently fell off prior to the PCD inspection, the areal loading of the residual cake is unknown. Therefore, it is not possible to calculate the PCD residual dustcake drag from the residual dustcake ΔP . However, the residual dustcake ΔP can be used in combination with the RAPTOR drag and the PCD face velocity to estimate the areal loading of the residual cake. Using an average RAPTOR drag value (at room temperature) of 100 inWC/(lb/ft²)/(ft/min), a residual dustcake ΔP of 29 inWC (at room temperature), and a face velocity of 3.5 ft/min, the areal loading of the residual cake is estimated to be 0.08 lb/ft². This value of areal loading is much higher than the areal loading that was estimated from the measured thickness, confirming that much of the residual cake fell off. The calculated areal loading is somewhat lower than the areal loading that was measured for GCT4, where the residual cake was held together with tar. This result suggests that tar deposition can contribute to the formation of a thicker residual dustcake and consequently a higher baseline ΔP , but no such effect was evident in TC06.

3.4.7 Real-Time Particulate Monitor Evaluation

As discussed in the GCT3 and GCT4 reports, testing of the PCME Dustalert-90 electrodynamic particulate monitor indicated that this device might have the potential to detect PCD leaks at levels low enough for turbine protection. During GCT4, the monitor responded to injected combustion ash particles in a definite, repeatable way with ash concentrations in the range of approximately 8 to 30 ppmw. The goal of the TC06 testing was to evaluate the response of the Dustalert-90 with g-ash as the injected particulate and at lower injected concentrations. To facilitate this testing, the dust injection system that has been described in previous reports was modified to operate at lower flow rates, so that lower concentrations of g-ash could be produced in the syngas downstream from the PCD. Because g-ash is more readily fluidized than ash, it was also necessary to increase the injection system fluid-bed disengager height and improve the fluidizing nitrogen distribution system to achieve reliable operation. With the modified injection system it was possible to test the response of the PCME monitor over a range of g-ash concentrations from about 0.5 to 3 ppmw.

The Dustalert-90 results from TC06 are shown in [Figure 3.4-9](#), which is a plot of actual particle concentration measured with the in situ sampling system as a function of the PCME monitor output. Since the Dustalert-90 does not determine particle concentration directly but instead measures the number of particles passing the probe per-unit time, and the gas flow during the measurement must be taken into account. The particle concentrations shown in the figure have been normalized to a syngas flow of 25,000 lb/hr. The five data points at the lower concentrations were obtained with injected g-ash while the one point at the highest concentration was determined during the leak that occurred at the end of TC06A. The line on the graph is a linear regression to all of the data. Although the correlation is not very good ($r^2 = 0.88$), both the injected and leaked g-ash values appear to follow the same trend. This is encouraging because of concerns that this instrument might respond differently to injected g-ash than it does to particles straight from the Transport Reactor.

The most promising result from the TC06 tests of the Dustalert-90 is that a clear indication was obtained from the instrument at injected concentrations as low as 0.5 ppmw. This is a sufficiently low concentration to provide a significant level of turbine protection. We will continue to refine our understanding of this instrument during future test programs.

3.4.8 Conclusions

The g-ash entering the PCD during TC06 was very similar to the g-ash produced during GCT4 (uncompacted bulk porosity of about 88 percent, specific-surface area of about 200 m²/g, and mass-median diameter of about 15 μm). Despite this similarity in the inlet g-ash, the residual dustcakes and the bridged deposits from TC06 have significantly higher porosities and higher surface areas than do the same types of samples from GCT4. These differences reflect the effect of tar deposition within the GCT4 dustcakes and deposits. Since the properties of the TC06 dustcakes and deposits are also similar to the properties of the TC06 in situ samples, any effect of tar deposition within the TC06 dustcake appears to be minimal. The use of coke feed during periods of interrupted coal feed was apparently successful in minimizing tar formation.

Throughout all of TC06B and most of TC06A, the PCD operated with outlet particulate loadings below the lower limit of resolution (0.1 to 0.4 ppmw). The only exception to the excellent particulate collection performance occurred after a thermal excursion led to a cracked filter element. This thermal excursion was caused by a situation that would not occur in a commercial facility.

Drag and surface area measurements made on TC06, GCT4, and GCT2 g-ash samples suggest that tar deposition can have a significant effect on the drag of high-surface-area g-ashes and very little effect on the drag of low-surface-area g-ashes. These measurements also support the conclusion that the residual dustcake from TC06 was relatively free of tar. Laboratory drag measurements made on hopper samples and bridged deposits were in good agreement with transient drag values calculated from the rate of ΔP rise, again suggesting that the transient dustcake drag was not affected by tar deposition.

Testing of the PCME Dustalert-90 real-time particulate monitor with injected g-ash suggests that the monitor is capable of detecting g-ash concentrations as low as 0.5 ppmw in the process gas stream downstream from the PCD (based on a syngas-flow rate of 25,000 lb/hr). Based on comparisons with batch measurements, the response of the monitor appears to be directly proportional to the mass-flow rate of g-ash in the process pipe. Additional testing is needed to validate the performance of the monitor on actual PCD leaks and to determine how the response of the monitor varies with different types of g-ash.

Table 3.4-1
 PCD Inlet and Outlet Particulate Measurements From TC06

Test Date	PCD Inlet				PCD Outlet					PCD Collection Efficiency, %
	SRI Run No.	Start Time	End Time	Particle Loading, ppmw	SRI Run No.	Start Time	End Time	H ₂ O Vapor, vol. %	Particle Loading, ppmw	
TC06A										
07/11/01	1	08:00	08:10	7,400 ¹	--	--	--	--	--	--
07/12/01	3	12:45	13:15	7,000 ¹	--	--	--	--	--	--
07/16/01	4	10:30	10:45	11,600 ²	1	09:45	13:45	10.9	< 0.1	> 99.999
07/17/01	5	09:45	10:00	13,100	2	09:15	13:00	10.3	-- ³	> 99.999
07/18/01	6	10:00	10:10	14,900	3	09:30	13:30	9.6	< 0.1	> 99.999
07/19/01	7	10:15	10:25	10,600	4	09:30	13:25	8.4	< 0.1	> 99.999
07/20/01	8	09:35	09:45	18,800	5	08:45	11:45	7.6	< 0.1	> 99.999
07/23/01	9	10:10	10:20	14,200	6	10:05	13:05	7.1	< 0.1	> 99.999
07/24/01	--	--	--	--	7	09:10	10:10	8.0	1.2 ⁴	--
07/25/01	--	--	--	--	8	09:55	10:45	--	22.9 ⁵	--
TC06B										
08/20/01	--	--	--	--	9	13:15	14:15	4.6	< 0.4 ⁶	--
08/21/01	10	09:30	09:45	14,900	10	08:30	09:33	9.2	< 0.4 ⁶	> 99.997
08/23/01	11	11:00	11:15	14,100	11	10:50	12:15	6.7	< 0.4 ⁶	> 99.997
08/27/01	12	09:00	09:14	10,400	12	08:45	11:32	5.8	< 0.1	> 99.999
08/29/01	13	08:40	08:55	11,800	13	08:15	10:52	5.8	< 0.1	> 99.999
08/30/01	14	09:45	10:00	17,000	14	09:30	13:30	5.8	< 0.1	> 99.999
08/31/01	15	10:00	10:15	13,500	15	09:30	13:00	6.3	< 0.1	> 99.999
09/04/01	16	10:00	10:15	16,300	16	09:25	13:25	6.5	< 0.1	> 99.999
09/05/01	17	09:30	09:45	16,500	17	09:15	13:15	7.0	< 0.1	> 99.999
09/06/01	18	12:25	12:40	16,600	18	10:15	13:15	7.0	< 0.1	> 99.999
09/07/01	--	--	--	--	19	10:25	11:15	7.8	2.1 ⁴	--
09/07/01	--	--	--	--	20	13:33	14:03	8.4	2.7 ⁴	--
09/10/01	19	10:00	10:15	17,000	21	09:30	13:30	7.4	< 0.1	> 99.999
09/11/01	--	--	--	--	22	09:20	12:20	8.3	0.5 ⁴	--

continued on next page

Table 3.4-1

PCD Inlet and Outlet Particulate Measurements From TC06 (continued)

Test Date	PCD Inlet				PCD Outlet					PCD Collection Efficiency, %
	SRI Run No.	Start Time	End Time	Particle Loading, ppmw	SRI Run No.	Start Time	End Time	H ₂ O Vapor, vol. %	Particle Loading, ppmw	
09/12/01	20	09:45	10:00	14,000	23	09:00	13:00	7.9	< 0.1	> 99.999
09/13/01	21	10:40	10:55	11,700	24	10:30	13:30	8.6	< 0.1	> 99.999
09/14/01	25	10:30	12:00	7.3	1.6 ⁴	..
09/17/01	22	10:00	10:15	9,300	26	09:45	13:45	8.5	< 0.1	> 99.999
09/18/01	23	09:30	09:55	9,700	27	09:00	13:00	8.4	< 0.1	> 99.999
09/19/01	24	09:45	10:00	9,200	28	09:20	13:20	7.3	< 0.1	> 99.999
09/20/01	25	10:00	10:15	18,100	29	09:00	13:00	7.3	< 0.1	> 99.999
09/21/01	26	09:30	09:45	11,900	30	09:00	13:00	7.7	< 0.1	> 99.999
09/24/01	27	09:00	09:15	15,800	31	08:30	11:30	7.1	< 0.1	> 99.999
Average Inlet Loading				13,900	Average Outlet Loading				< 0.1	> 99.999

1. Inlet samples 1 and 3 collected during coke feed – not included in average. Inlet sample 2 discarded because of filter leakage.
2. Inlet sample 4 collected without limestone addition.
3. Filter weight problem with outlet sample 2 – measurement not reliable.
4. Outlet sample collected during dust injection for particulate monitor calibration – no PCD leak – not included in average.
5. Outlet sample 8 collected during propane combustion – PCD leak through cracked filter element.
6. Short duration test – resolution reduced accordingly.

Table 3.4-2

Physical Properties of TC06 In situ Samples¹

Lab ID	SRI Run No.	Date	Bulk Density, g/cm ³	True Density, g/cm ³	Uncompacted Bulk Porosity, %	Surface Area, m ² /g	Mass-Median Diameter, µm
<i>TC06A</i>							
AB08748	TC06IMT-1	07/11/01	0.48	2.17	77.9	16.7	18.9
AB08750	TC06IMT-3	07/12/01	0.50	2.26	77.9	10.2	19.1
AB08751	TC06IMT-4	07/16/01	0.31	2.49	87.6	182	18.6
AB08752	TC06IMT-5	07/17/01	0.34	2.67	87.3	151	13.1
AB08753	TC06IMT-6	07/18/01	0.32	2.63	87.8	180	12.7
AB08754	TC06IMT-7	07/19/01	0.24	2.35	89.8	257	13.1
AB08755	TC06IMT-8	07/20/01	0.27	2.43	88.9	215	14.7
AB08756	TC06IMT-9	07/23/01	0.31	2.46	87.4	197	14.3
<i>TC06B</i>							
AB09219	TC06IMT-10	08/21/01	0.31	2.51	87.6	183	15.1
AB09220	TC06IMT-11	08/23/01	0.33	2.41	86.3	145	18.6
AB09221	TC06IMT-12	08/27/01	0.29	2.35	87.7	221	14.2
AB09222	TC06IMT-13	08/29/01	0.29	2.42	88.0	255	16.2
AB09223	TC06IMT-14	08/30/01	0.27	2.52	89.3	219	16.1
AB09224	TC06IMT-15	08/31/01	0.29	2.60	88.8	248	16.7
AB09225	TC06IMT-16	09/04/01	0.28	2.40	88.3	244	18.1
AB09226	TC06IMT-17	09/05/01	0.24	2.27	89.4	310	14.6
AB09227	TC06IMT-18	09/06/01	0.27	2.41	88.8	262	15.2

continued on next page

Table 3.4-2

Physical Properties of TC06 In situ Samples (continued)¹

Lab ID	SRI Run No.	Date	Bulk Density, g/cm ³	True Density, g/cm ³	Uncompacted Bulk Porosity, %	Surface Area, m ² /g	Mass-Median Diameter, µm
AB09442	TC06IMT-19	09/10/01	0.27	2.39	88.7	266	12.5
AB09443	TC06IMT-20	09/12/01	0.24	2.32	89.7	311	11.4
AB09444	TC06IMT-21	09/13/01	0.32	2.62	87.8	202	18.3
AB09445	TC06IMT-22	09/17/01	0.36	2.60	86.2	135	15.4
AB09446	TC06IMT-23	09/18/01	0.27	2.39	88.7	195	16.2
AB09447	TC06IMT-24	09/19/01	0.32	2.43	86.8	187	16.4
AB09448	TC06IMT-25	09/20/01	0.26	2.28	88.6	243	16.8
AB09449	TC06IMT-26	09/21/01	0.26	2.33	88.8	243	16.5
AB09450	TC06IMT-27	09/24/01	0.22	2.40	90.8	277	13.0
TC06 Average ¹			0.29	2.45	88.3	222	15.3

1. Sample Nos. TC06IMT-1 and -3 collected during coke feed; not included in average.

Table 3.4-3

Physical Properties of TC06 Dustcake Samples¹

Lab ID	Type	Date	Bulk Density, g/cc	Particle Density, g/cc	Uncompacted Bulk Porosity, %	Surface Area m ² /g	Mass-Median Diameter, μ m
<i>TC06A</i>							
AB08757	Residual	07/27/01	0.46	2.62	82.4	4.6	5.7
AB08758	Residual	07/27/01	0.46	2.50	81.6	24.9	9.9
AB08759	Residual	07/27/01	0.47	2.58	81.8	24.8	14.2
AB08760	Deposit ²	07/27/01	0.53	2.68	80.2	24.4	11.1
<i>TC06B</i>							
AB09474	Bridging	09/27/01	0.27	2.41	88.8	261	10.8
AB09475	Transient	09/27/01	0.25	2.39	89.5	261	9.2
AB09476	Residual	09/27/01	0.25	2.28	89.0	257	9.3

1. TC06A dustcake samples appear to have been partially combusted as a result of fire in PCD.
2. Deposit removed from filter element support bracket.

Table 3.4-4

Transient Drag Determined From PCD ΔP and From RAPTOR

Run No.	$\Delta P/\Delta t$, inWC/min	$\Delta(AL)/\Delta t$, lb/min/ft ²	FV, ft/min	MMD, μm	Drag, inWC/(lb/ft ²)/(ft/min)		
					PCD	PCD@RT	RAPTOR
5	8.46	0.02440	3.67	13.1	94	57	104
6	10.49	0.02748	3.63	12.7	105	63	107
8	14.65	0.03496	3.71	14.7	113	68	94
9	12.55	0.02604	3.67	14.3	131	79	96
10	10.48	0.02521	3.68	15.1	113	68	91
11	13.27	0.02250	3.46	18.6	171	103	76
14	7.93	0.02660	3.18	16.1	94	57	86
15	9.67	0.02142	3.22	16.7	140	86	84
16	12.04	0.02788	3.53	18.1	122	74	78
17	15.73	0.02606	3.21	14.6	188	115	94
18	11.01	0.02699	3.29	15.2	124	75	91
19	14.39	0.02828	3.39	12.5	150	92	108
20	11.33	0.02092	2.96	11.4	183	114	117
25	7.76	0.02758	2.64	16.8	107	66	83
27	19.01	0.02778	3.18	13.0	215	131	104

Nomenclature:

1. $\Delta P/\Delta t$ = rate of pressure drop rise during particulate sampling run (inWC/min).
2. $\Delta(AL)/\Delta t$ = rate of increase in areal loading during sampling run (lb/min/ft²).
3. FV = average PCD face velocity during particulate sampling run (ft/min).
4. MMD = mass-median diameter of in situ particulate sample (μm).
5. RT = room temperature, 77°F (25°C).
6. RAPTOR = resuspended ash permeability tester.

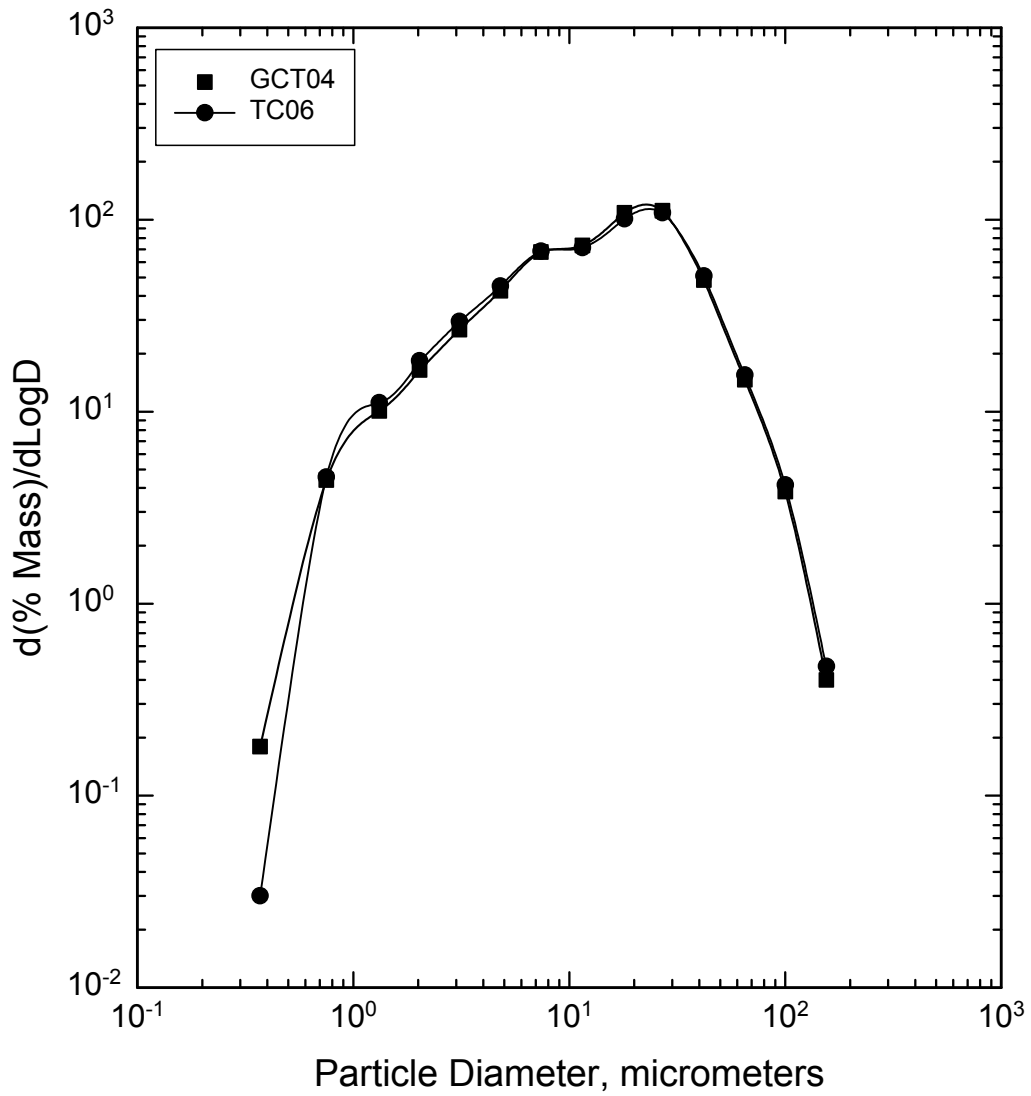


Figure 3.4-1 GCT4 and TC06 Coal G-ash Particle-Size Distributions

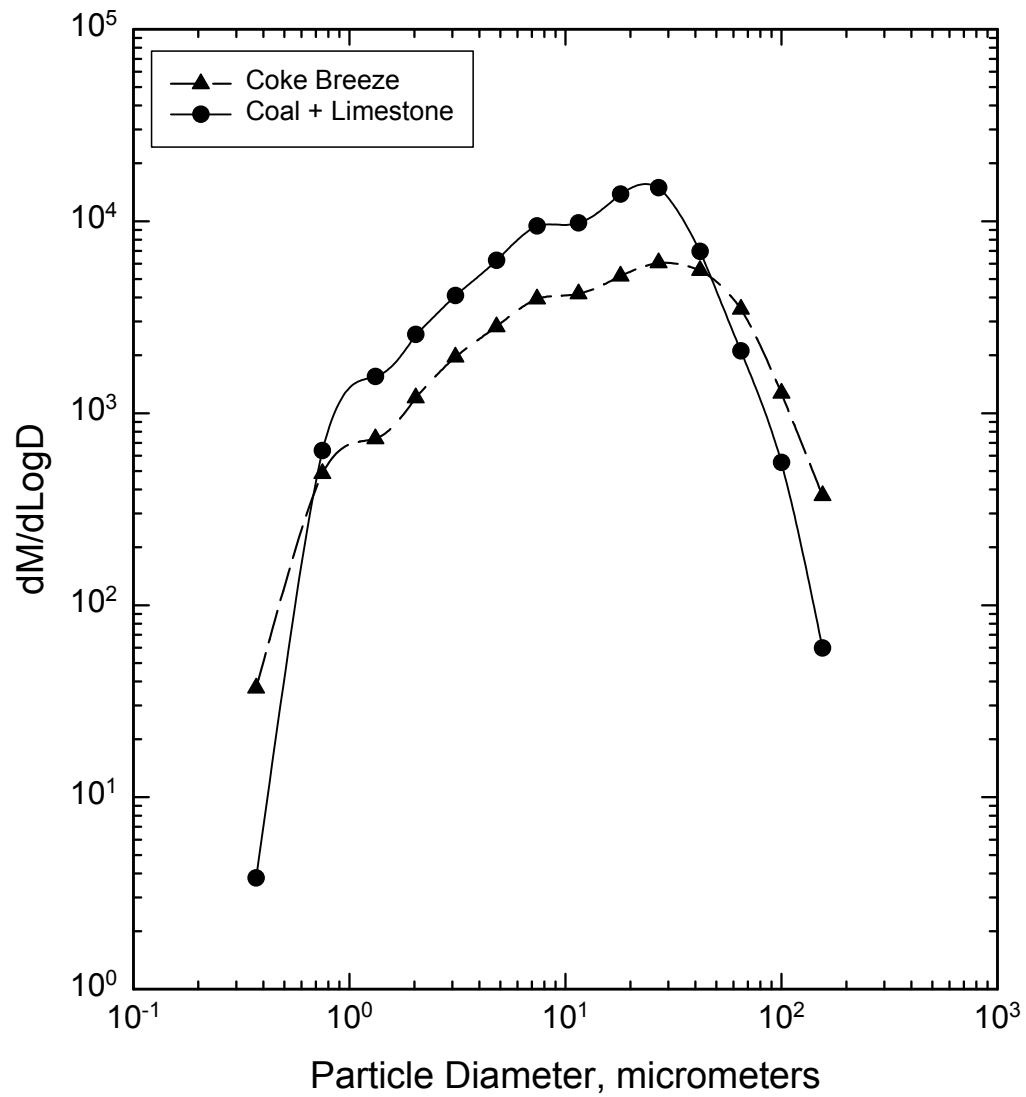


Figure 3.4-2 Particle-Size Distributions for Coal and Coke Operation

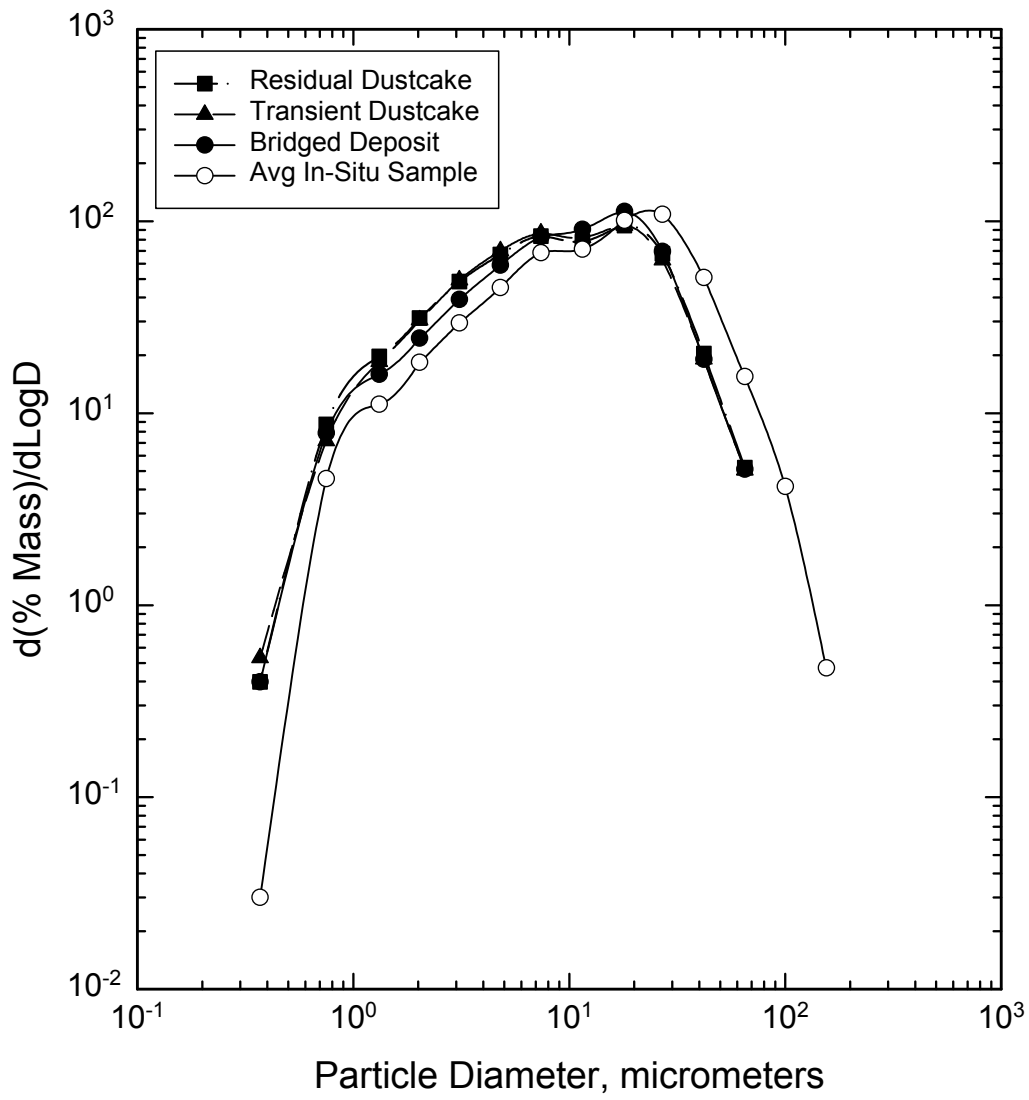


Figure 3.4-3 G-ash Particle-Size Distributions

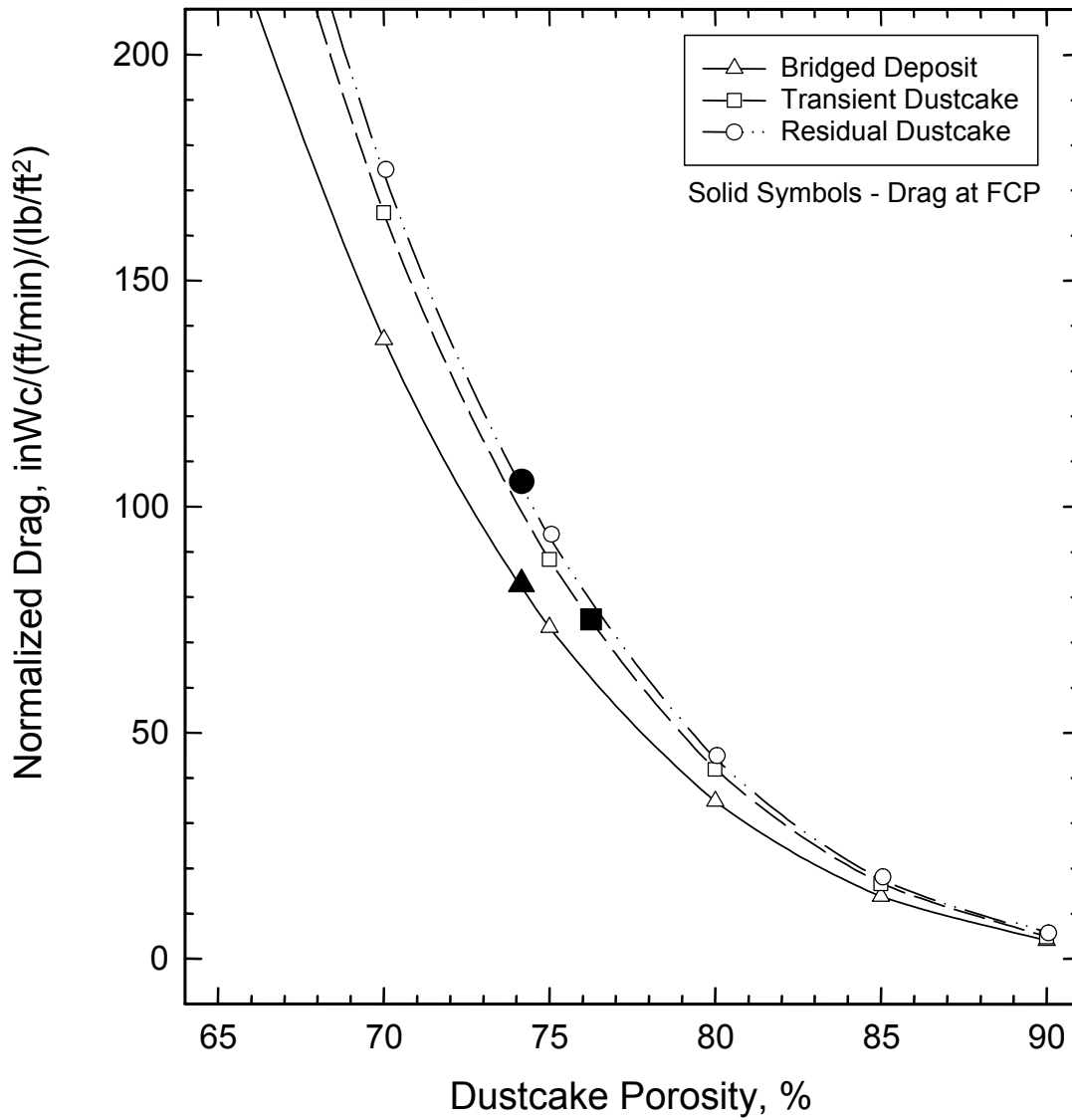


Figure 3.4-4 CAPTOR Drag of PCD Dustcake Samples (FCP Is the Flow-Compacted Porosity)

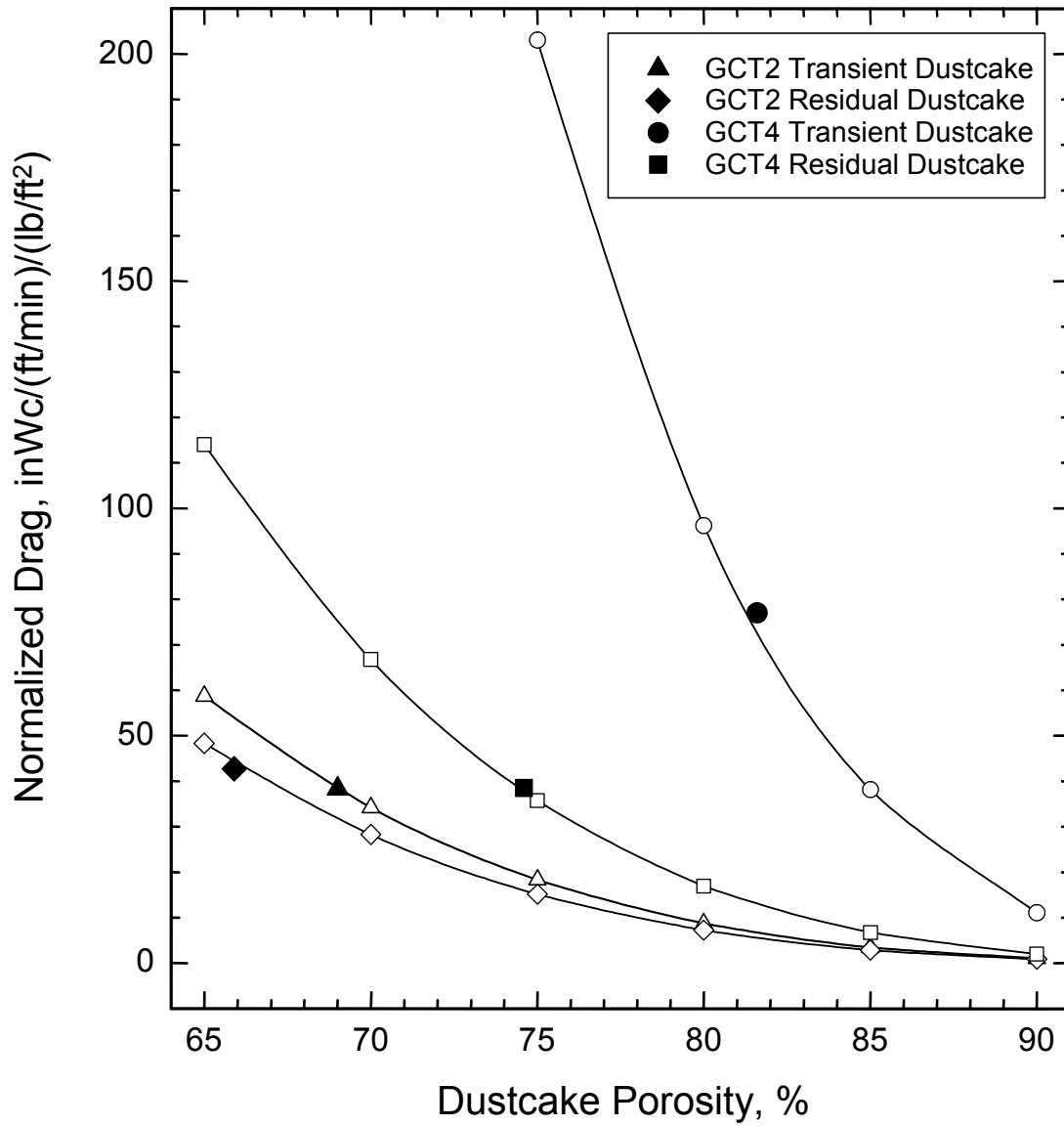


Figure 3.4-5 CAPTOR Drag During Previous Test Programs (Solid Symbols Denote Drag Measured at the Flow-Compacted Porosity)

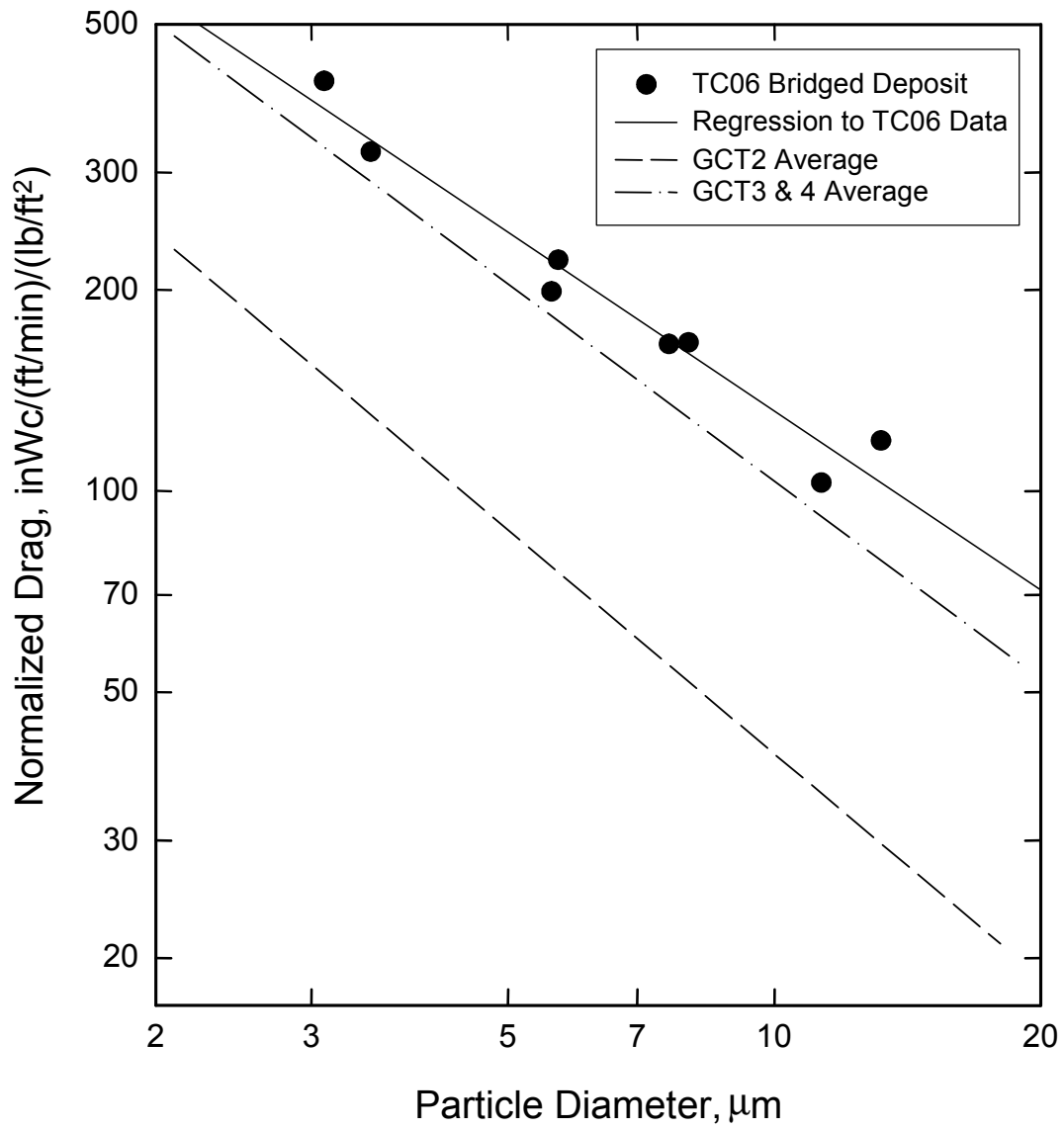


Figure 3.4-6 G-ash Drag as a Function of Particle Size

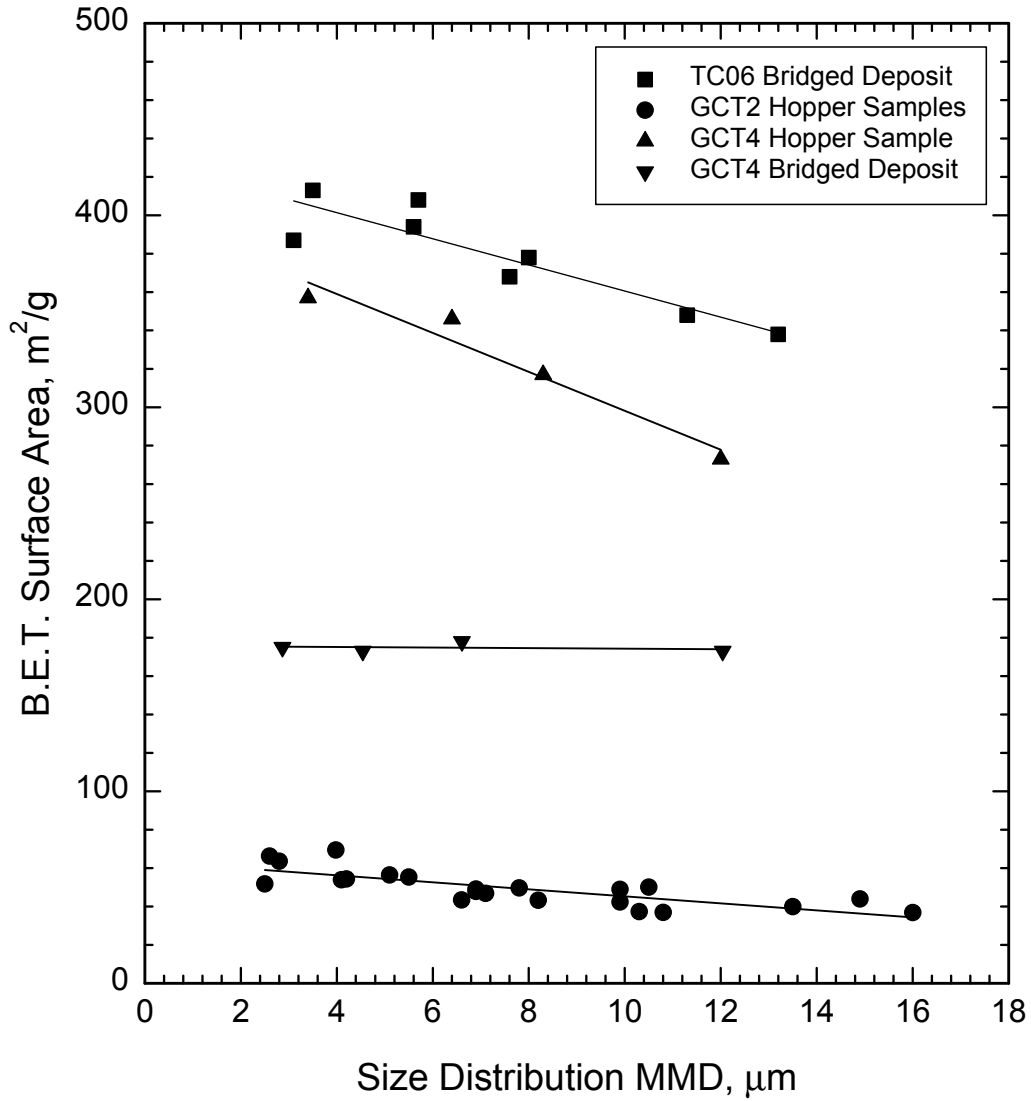


Figure 3.4-7 BET Surface Areas of G-ash Samples

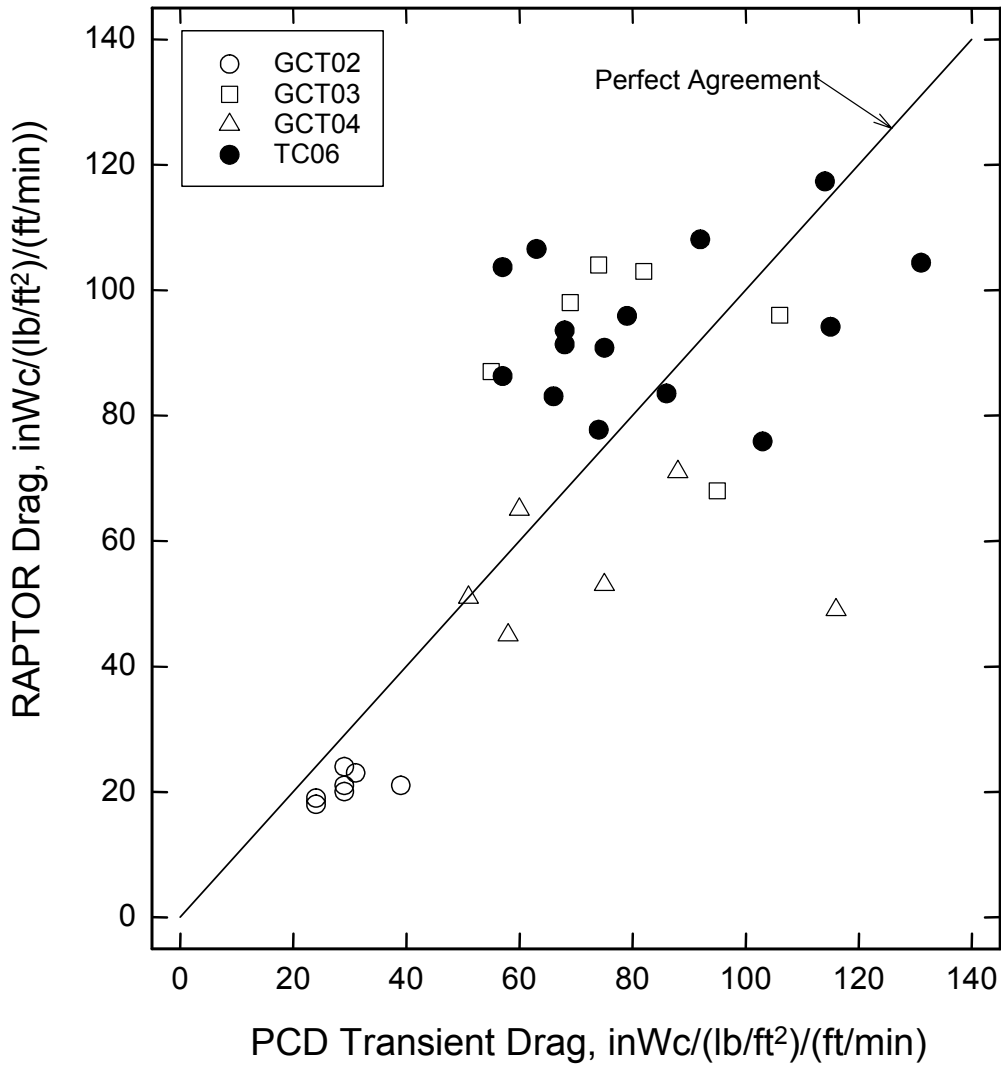


Figure 3.4-8 Comparison of Actual PCD Drag With RAPTOR Estimated Drag

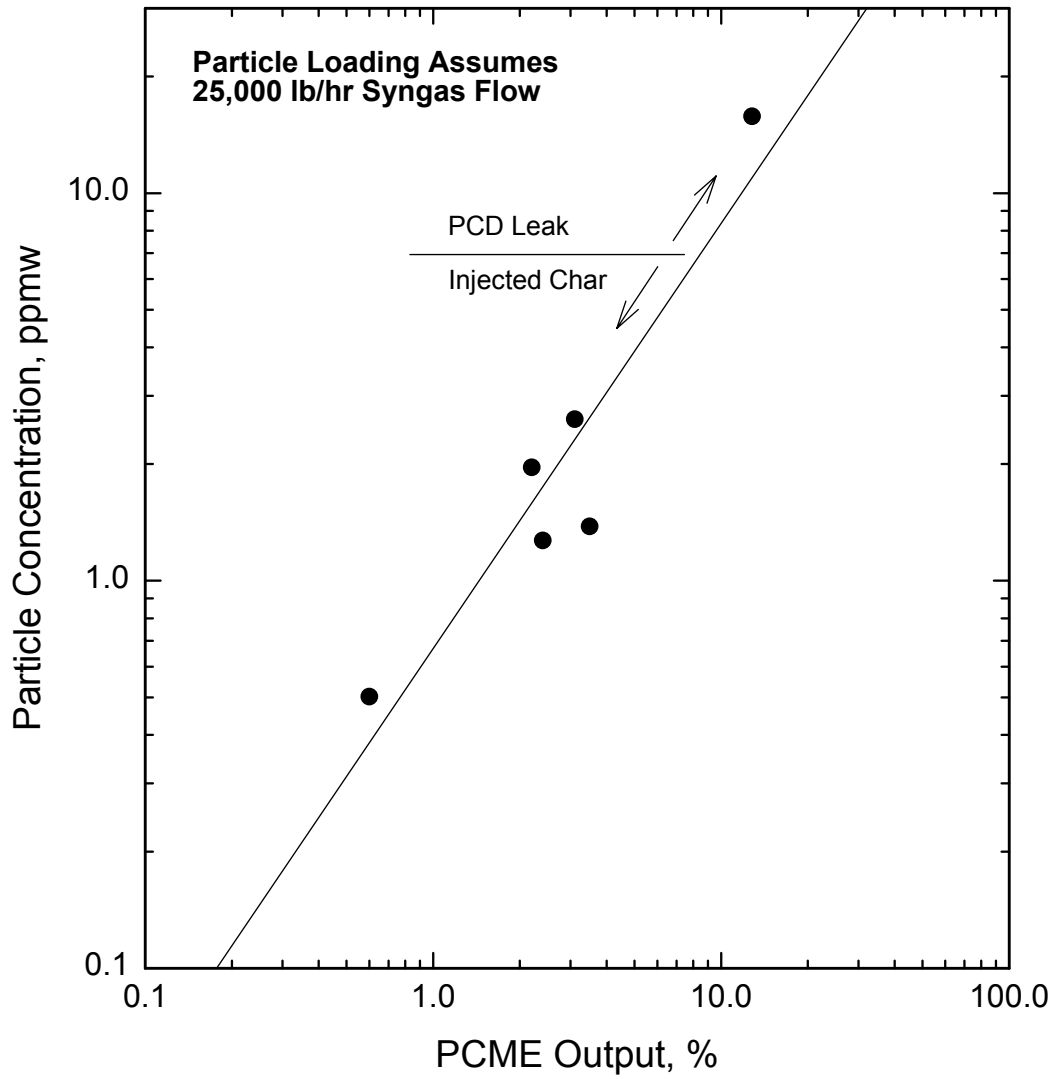


Figure 3.4-9 Calibration Tests on PCME Dustalert-90 Real-Time Monitor

3.5 TEST RESULTS FOR FILTER ELEMENTS

Property testing of filter elements continued during this test campaign. Pall iron aluminide (Fe_3Al), Schumacher T10-20, and Pall 326 elements were tested. The elements tested and their operational histories are summarized in [Table 3.5-1](#). The test plan for each individual element is summarized in the test matrices shown in [Tables 3.5-2](#) and [-3](#). Specimens required to conduct the testing were removed from the elements as shown on the cutting plans in [Figures 3.5-1](#) to [-6](#).

The GCT3 test run was a 184-hour gasification run with a nominal operating temperature of 700°F. There was a thermal transient during this run where 14 thermocouples in the PCD vessel, which are mounted near the outside surfaces of the elements, measured a temperature increase of approximately 300°F in 1 minute. One Schumacher T10-20 element and one Pall 326 element were removed after this run and tested to determine if they suffered damage during the thermal transient. Fe_3Al element 27056 was also tested after this run. GCT4 was a 242-hour gasification run with a nominal operating temperature of 700°F. Fe_3Al Element 27060 was tested after operation in both GCT3 and GCT4, 425 total hours of on-coal operation. TC06A was a 228-hour gasification run with a nominal operating temperature of 700°F. This run ended because particulate was detected downstream of the PCD following a thermal transient. The thermal transient was severe but localized. The temperature of the elements probably exceeded 1,800°F but only 15 elements were affected. Element 21076, which was cracked after TC06A (see photograph, [Figure 3.3-4](#)), was tested and examined microscopically. This thermal transient is discussed in greater detail in Section 3.3. Finally, Fe_3Al element 034H-005, with 2,780 hours of combustion operation at a nominal temperature of 1,450°F, was tested. This is the longest exposure time on any Fe_3Al element and it was tested to determine if any degradation occurred even though the current operating mode is gasification with a nominal operating temperature of 750°F. This element was in operation during thermal transients in TC03 and TC04 that caused some ceramic element failures.

3.5.1 Pall Fe_3Al

All room-temperature tensile stress-strain responses obtained so far for Fe_3Al elements from gasification operation are shown in [Figures 3.5-7](#) and [-8](#) for the axial and hoop directions, respectively. Axial stress-strain responses measured at 1,400°F are shown in [Figure 3.5-9](#). The hoop and axial tensile strengths are plotted versus hours in operation in [Figure 3.5-10](#). All results are summarized in [Tables 3.5-4](#) and [-5](#). The hoop stress-strain responses (see [Figure 3.5-8](#)) represent the strains measured on the outside surface of the specimens and the corresponding stresses at the outside surface. However, for this test the specimens were loaded by hydrostatic pressure at the inside surface and the maximum stresses and strains occur at the inside surface. Therefore, the endpoints of these curves do not represent ultimate strength or strain values. The tensile strengths measured on virgin elements and after 63 hours were ~10 percent greater than the strengths measured after 180 to 650 hours; however, the hydrostatic burst pressure was nearly the same. This is because of variations in wall thickness. The elements tested in virgin condition and after 63 hours had thinner walls so the tensile stress was greater for the same hydrostatic pressure. In the axial direction, the strength was ~5 to 15 percent lower after operation than on virgin material; however, there have not been enough elements tested so far to assess element-to-element strength variation. The slightly lower

strength may be because of material variability, not a strength decrease during operation. The 0.05-percent yield strength (a line was drawn parallel to the initial slope of the stress-strain curve but offset by 0.0005 and the intersection of this line with the stress-strain curve is the 0.05-percent yield strength) also did not change after operation. Elevated temperature tensile strengths, in the axial direction only, were also slightly lower on the elements tested after operation. Again, this may be because of material variability. It is important to note that all Fe₃Al elements tested after gasification operation, with the possible exception of element 034H-004 tested after 63 hours in GCT1A, were in operation during at least one thermal transient event. As discussed in the second paragraph of Section 3.5, the severity of the thermal transients varied. There was a thermal transient during GCT1A with a temperature increase of ~135°F in 7.5 minutes measured on one element. There was no thermocouple on element 034H-004; therefore, it is not known if this element was affected by the thermal transient. The strengths may have been affected by the thermal transients as well as by normal operation. Because Fe₃Al has high thermal conductivity, thin walls, and high strain-to-failure compared to the Pall and Schumacher clay-bonded SiC, it was assumed that thermal transients survived by the clay-bonded SiC elements would have little or no effect on Fe₃Al elements. However, this has not been verified.

Hoop tensile results from element 21076, which was cracked during the thermal transient of TC06A, indicated that the tensile strength of 2 of 3 specimens was near the strength of all other specimens tested after operation. The other specimen from this element had strength ~18 percent below these two specimens. This could have been because of either material variability or damage from the transient. All specimens failed along the line separating the region of the element that was exposed to the highest temperature increase as shown in [Figure 3.5-11](#). Results from this element indicate that there may have been local areas of damage that caused lower strength while the overall strength of the element was not affected.

Two room-temperature axial specimens, Tn-Ax-16 and 20, from element 27056, removed from operation after GCT3, had ultimate strengths and strains-to-failure significantly lower than all other axial tensile specimens. Examination of the fracture surfaces showed these two specimens had pits or voids that were barely visible unaided and easily seen with a low-powered optical microscope. SEM images of two regions on the fracture surface of specimen Tn-Ax-16 are shown in [Figures 3.5-12](#) and [-13](#). Similar regions were also seen on specimen Tn-Ax-20. Pitting was seen in each of these regions, both at the surface and internally. Higher magnification images of two selected pits, locations A and B in [Figure 3.5-13](#), are shown in [Figures 3.5-14](#) and [-15](#). An image from a typical region of a specimen with no pits, Tn-Ax-22, is shown for comparison at the higher magnification in [Figure 3.5-16](#). Particle size and morphology were both different in the pits than the material away from the pits. The particles inside of the pits were larger and had smoother edges. Elemental compositions were also different. Spectra obtained by energy dispersive spectroscopy (EDS) are shown in [Figures 3.5-17](#) to [-19](#) for the regions pictured in [Figures 3.5-14](#) to [-16](#), respectively. The typical composition shown in [Figure 3.5-19](#) was iron, aluminum, and chromium. At many locations, oxygen was also seen although it does not appear in the spectra shown in [Figure 3.5-19](#). Spectra from the pits, [Figures 3.5-17](#) and [-18](#), show large peaks representing the presence of chlorine. Chlorine was found in all pits but was not detected at any locations away from the pits. There were other “foreign” elements including sulfur, calcium, lead, arsenic, and titanium found in some, but not